

DIPLOMARBEIT

Atmospheric Impact on Laser Beam Propagation

ausgeführt am Institut für
Nachrichtentechnik und Hochfrequenztechnik der
Technischen Universität Wien
von

Bernhard Dehlink

Magdalenengasse 13
2540 Bad Vöslau

Matrikelnummer 9825109

Wien, im April 2004

Betreuer:

Dr. Martin Pfennigbauer
Prof. Dr. Walter R. Leeb

Danksagung

Herzlicher Dank gilt allen, die mich bei der Entstehung dieser Arbeit unterstützt haben. Ganz besonders bedanke ich mich bei:

Herrn Prof. Dr. Walter R. Leeb, Vorstand des Instituts für Nachrichten- und Hochfrequenztechnik, für die Möglichkeit der Durchführung der Diplomarbeit und für viele interessante Diskussionen.

Vor allem bei meinem Betreuer, Herrn Dr. Martin Pfennigbauer, für die hervorragende Betreuung und konstruktive Kritik, sowie für zahlreiche Ratschläge und motivierende Worte.

Herrn Dr. Oswald Wallner für die bereitwillige Unterstützung bei der Bewältigung von mathematischen und technischen Problemen.

Meiner Mutter Mag. phil. Brigitta, meinem Vater DI Dr. techn. Alois, meiner Schwester Dr. med. Eleonora Dehlink und meiner Lebensgefährtin Elisabeth Riegler, sowie meiner ganzen Familie und allen lieben Freunden, die mich während meines gesamten Studiums unterstützt haben.

Abstract

Free-space laser communication systems are an excellent choice when high data rates are demanded. The outstanding cause for the advantages of an optical system over radio frequency technology is the low beam divergence. Within this thesis, the atmospheric impacts on optical Earth-to-Satellite communication links are investigated.

Certain restrictions arise when lasers are employed within free-space transmission links: The atmosphere absorbs optical power and affects the shape of the beam. It has to be expected that the beam is displaced (beam wander), that the divergence is increased further than in the diffraction limited case (beamspread), and that the angle of arrival of the laser beam at the receiver varies. The phase front is distorted, leading to intensity variations at the receiver (scintillations). These phenomena result in a loss of power, or in a link failure in the worst case. While I analyze the aforementioned impacts in detail, absorption effects are treated only briefly within this thesis.

The variations in the refractive index of air is the governing property of free-space laser beam propagation. Wind and temperature gradients cause the air to be in permanent motion. I arrive at the decision that the atmospheric structure must be considered turbulent, so a stochastic description of the refractive index is indispensable. It is necessary to solve the wave equation for the analysis of the properties of a laser beam, but it is not possible to solve this equation directly when a stochastic refractive index is utilized. I choose statistical moments of different order for further calculations. Closed form solutions only exist for moments of the lowest order, thus approximations have to be employed. I present different methods, and focus on the *Rytov approximation* and the *Markov approximation*. These methods differ in the mathematical approach to the solution for the statistical moments.

I use the Rytov and the Markov approximation method to analyze the atmospheric impacts on an Earth-Satellite link. As an example, the satellite being investigated is orbiting at the low earth orbit (450 km), and the wavelength of the laser beam is $1.55\text{ }\mu\text{m}$. I show that the beam wander will be on the order of approximately 1.5 m, and that the diameter of the beam is expected to be three times the diffraction limited diameter. The fluctuations of the arrival angle amount to a few microradians, thus will be negligible. These results apply to the uplink case only, it is shown that the atmosphere is negligible in the downlink case. The results are roughly the same for both methods.

I show that the additional link loss due to the atmosphere must not be neglected. It is essential to employ a fast tracking system at the transmitter and the receiver to prevent the loss of the signal.

Kurzfassung

Optische Übertragungssysteme zeichnen sich durch die Möglichkeit der Realisierung sehr hoher Datenraten aus. Der Grund dafür liegt im verwendeten Frequenzbereich, der eine hohe Bandbreite zulässt. Als weitere Konsequenz der optischen Frequenzen ergibt sich eine sehr kleine Aufweitung des Strahls. Während dies einer der größten Vorteile der optischen Kommunikation ist, ergeben sich Probleme wenn es große Distanzen zu überbrücken gilt, wie etwa bei der Kommunikation zwischen einer Bodenstation und einem Satelliten. In dieser Diplomarbeit werden die Auswirkungen der Atmosphäre auf die Ausbreitung von Laserstrahlen behandelt.

Bei optischen Freiraumkommunikationssystemen kommt es, stärker als bei Funksystemen, zu Nachteilen durch das Medium, in dem sich der Laserstrahl ausbreitet: Die Atmosphäre absorbiert einerseits einen Teil der Leistung, andererseits wird auch die Strahlform verändert. Es ist zu erwarten, dass der Strahl durch die Atmosphäre abgelenkt wird und dass er sich zusätzlich verbreitert. Ebenfalls wird der Winkel, unter dem der Strahl am Empfänger auftrifft, nicht konstant sein. Durch die Atmosphäre treten Verzerrungen der Phasenfront auf, die zu lokalen Fluktuationen des Feldbildes, folglich zu Intensitätsschwankungen, führen. All diese Phänomene tragen dazu bei, dass am Empfänger weniger Leistung vorhanden ist als ohne Atmosphäre.

Die Ursache für die Änderungen der Eigenschaften eines Laserstrahls liegt in den Variationen des Brechungsindex der Luft. Durch Druck- und Temperaturgradienten stellt sich eine turbulente Struktur der Atmosphäre ein, was wiederum zu einer zufälligen Verteilung des Brechungsindex führt. Folglich ist eine mathematische Beschreibung des Brechungsindex nur mit stochastischen Mitteln möglich. Um nun die Auswirkungen der Atmosphäre auf die Ausbreitung von Laserstrahlen zu quantifizieren, muss die Wellengleichung (die den stochastischen Brechungsindex enthält) gelöst werden. Dies ist mit einfachen Mitteln nicht möglich. Ich entscheide mich, durch die Verwendung von statistischen Momenten, dieses Problem zu umgehen. Für die Berechnung der Momente ist es notwendig, Näherungen einzuführen. Im Speziellen konzentriere ich mich auf zwei Methoden, die *Rytovnäherung* und die *Markovnäherung*.

Durch die Verwendung dieser Näherungen ist mir die Analyse des Einflusses der Atmosphäre auf eine Datenverbindung zwischen der Erde und einem Satelliten möglich. Als Fallbeispiel ziehe ich einen Satelliten heran, der in einer Höhe von 450 km die Erde umkreist. Die Wellenlänge für die Kommunikation beträgt $1.55\text{ }\mu\text{m}$. Es stellt sich heraus, dass der Laserstrahl im Fall der Aufwärtsstrecke ("Uplink") um bis zu 1.5 m abgelenkt wird, und dass der Durchmesser des Strahls um das Dreifache gegenüber dem beugungsbegrenzten Fall aufgeweitet wird. Vernachlässigbar sind die schnellen Variationen im Ankunftswinkel, die einige Mikroradian betragen. Diese Ergebnisse werden sowohl von der Rytovnäherung als auch von der Markovnäherung erzielt. Es bestehen gravierende Unterschiede zwischen der Aufwärts- und der Abwärtsstrecke. Alle genannten Abschätzungen beziehen sich auf die Strecke von der Erde zum Satelliten, für den Fall der Kommunikation vom Satelliten zur Erde ist die Atmosphäre vernachlässigbar.

Durch die enorme Ablenkung des Strahls erweist sich der Einsatz von schnellen Nachführungssystemen als unerlässlich. Für einfachere Systeme lassen sich große Dämpfungsfaktoren, die bis zum Verlust des Signals führen können, nicht ausschließen.

Contents

1	Introduction	1
2	Beam Profiles	3
2.1	Plane Waves	4
2.2	Spherical Waves	5
2.3	Gaussian Beam	6
3	Waves in Random Media	10
3.1	Index of Refraction	10
3.2	Moments of the Field	12
3.3	Solutions for the Stochastic Wave Equation	13
3.3.1	Direct Solution Methods	13
3.3.2	Geometrical Optics Method	15
3.3.3	Born Approximation	16
3.3.4	Rytov Approximation	17
3.3.5	Markov Approximation	20
4	Laser Beam Propagation in the Atmosphere	23
4.1	Topology of the Atmosphere	23
4.2	Turbulence	25
4.3	Structure Functions	27
4.4	Spectra of Turbulence	30
4.4.1	The Structure Parameter C_n^2	33
4.5	Classification of the Turbulent Environment	36
5	Results	38
5.1	Absorption	38
5.2	Scattering	38
5.3	Beam Wander	39
5.4	Short-Term Beamspread	42
5.5	Long-Term Beamspread	43
5.6	Other Impacts	47
6	System Loss	49
6.1	Overall Path Attenuation	49
6.2	Compensation of Atmospheric Impacts	52
6.3	Assessment	53

Appendices	55
Bibliography	59

Chapter 1

Introduction

The cause for the outstanding advantages of an optical communication system lies within the low divergence of the involved laser beam. For a satellite link from ground to space, the beam has to pass through the atmosphere. This particular medium decreases the intensity in two ways,

1. The *chemical elements* of air absorb the optical power. Most of the power is absorbed by water vapor. In addition, small particles in the air deflect the laser beam, increasing the attenuation factor.
2. Even for clear air (i.e., chemical elements do not have an impact on the laser beam), the atmospheric environment must not be neglected. The refractive index of air varies in time and space because of temperature and pressure inequalities. These variations are a result of the *structure of the atmosphere* that turns out to be *turbulent*.

The attenuation factor due to the first point is assumed to be negligible (some 1–2 dB during a sunny day or a clear night, for example). If this were not the case, the absorption will be so high that any optical link between the earth and a satellite can be expected to fail.

The more challenging part is the attenuation due to atmospheric turbulence. The turbulent environment leads to an additional broadening of the laser beam among other impacts. These impacts can only be described by stochastic means.

The aim of this diploma thesis is the analysis of atmospheric impacts on a laser beam for ground to space communication systems and a clear atmospheric environment, i.e., absorption is negligible. This thesis is organized as follows:

- Laser beams are electromagnetic waves that are well described by Gaussian beams. This particular type of beam is derived as a solution for the wave equation in Chapter 2.
- The governing property of a medium that changes the behavior of laser beams is the medium's index of refraction. Chapter 3 is dedicated to different types of solutions for the wave equation, involving stochastic refractive indices. (The atmosphere's refractive index is a stochastic field.)
- In Chapter 4, the topology and the structure of the atmosphere are introduced. Mathematical utilities that represent the refractive index of the atmosphere are presented.

- The diverse impacts on a laser beam propagating through atmospheric turbulence are outlined in Chapter 5. Two methods from Chapter 3 (Rytov approximation and Markov approximation) and results from Chapter 4 are combined to assess the order of magnitude of the atmospheric influence.
- The link attenuation for a specific earth-to-space communication scenario is calculated in Chapter 6. Methods to decrease the attenuation are suggested. A worst case estimation leads to a conclusion for the dynamic range of the attenuation.

The investigation of laser beam propagation through free-space as well as through random media requires a mathematical model for that type of the waves. That is the reason why I will start my analysis from scratch, in other words, with Maxwell's equations.

Chapter 2

Beam Profiles

In this chapter, the basics for the analysis of wave propagation are presented. Maxwell's equations are used as fundamentals for calculations involving electrodynamics, therefore they will be the starting point for the description of wave propagation, leading to the wave equation. Three commonly used types of solutions for the wave equation are introduced: the Plane Wave, the Spherical Wave, and the Gaussian beam. The focus will be laid on the Gaussian beam because this type of solution will be extensively used in the next chapters.

Maxwell's equations establish a relationship between the electric and the magnetic field, $\vec{\mathcal{E}}(\vec{x}, t)$ and $\vec{\mathcal{H}}(\vec{x}, t)$ respectively, at a fixed point in time and space. The following equations are not the original ones¹, but a simplified form² found by O. Heaviside and W. Gibbs (1884) in the cartesian coordinate system ($\vec{x} = x\vec{e}_x + y\vec{e}_y + z\vec{e}_z$, t represents the time):

$$\vec{\nabla} \cdot \varepsilon \vec{\mathcal{E}}(\vec{x}, t) = 0 \quad (2.1)$$

$$\vec{\nabla} \cdot \mu \vec{\mathcal{H}}(\vec{x}, t) = 0 \quad (2.2)$$

$$\vec{\nabla} \times \vec{\mathcal{E}}(\vec{x}, t) = \mu \frac{\partial \vec{\mathcal{H}}(\vec{x}, t)}{\partial t} \quad (2.3)$$

$$\vec{\nabla} \times \vec{\mathcal{H}}(\vec{x}, t) = -\varepsilon \frac{\partial \vec{\mathcal{E}}(\vec{x}, t)}{\partial t} \quad (2.4)$$

The vectorial differential operator Nabla ($\vec{\nabla}$) is defined as $\vec{\nabla} = \partial_x \vec{e}_x + \partial_y \vec{e}_y + \partial_z \vec{e}_z$, ε is the electric permittivity, and μ is the magnetic permeability. In vacuum, $\varepsilon = \varepsilon_0 = 8.856 \cdot 10^{-12} \frac{As}{Vm}$, and $\mu = \mu_0 = 4\pi \cdot 10^{-7} \frac{Vs}{Am}$.

It is possible to merge these coupled equations to get one expression for the electric field (the derivation for the magnetic field is analogue) by taking the curl of (2.3) and inserting (2.1), (2.4) [1]:

$$\nabla^2 \vec{\mathcal{E}}(\vec{x}, t) + \mu \varepsilon \frac{\partial^2 \vec{\mathcal{E}}(\vec{x}, t)}{\partial t^2} = 0. \quad (2.5)$$

In (2.5), the identity $\vec{\nabla} \times (\vec{\nabla} \times \vec{a}) = \vec{\nabla}(\vec{\nabla} \cdot \vec{a}) - \nabla^2 \vec{a}$ was used, where ∇^2 is the LAPLACE-OPERATOR in cartesian coordinates,

$$\nabla^2 = \frac{\partial^2}{\partial x^2} + \frac{\partial^2}{\partial y^2} + \frac{\partial^2}{\partial z^2}. \quad (2.6)$$

¹The original formulation was in terms of 20 equations in 20 variables.

²The following simplifications for dielectric materials are used: charge density, current density, and magnetization are negligible, thus set to zero.

Using the Maxwell relation,

$$c^2 \varepsilon \mu = 1, \quad (2.7)$$

the phase velocity c can be inserted into (2.5), and the result is the well-known wave equation in the case of an isotropic and linear medium:

$$\nabla^2 \vec{\mathcal{E}}(\vec{x}, t) + \frac{1}{c^2} \frac{\partial^2 \vec{\mathcal{E}}(\vec{x}, t)}{\partial t^2} = 0. \quad (2.8)$$

To simplify further calculations, the next objective is to separate the time-dependency and the space-dependency of $\vec{\mathcal{E}}(\vec{x}, t)$. Considering only time-harmonic oscillating functions, which is no limitation to the applications treated here, this step can be taken easily:

$$\vec{\mathcal{E}}(\vec{x}, t) = \Re \left[\vec{E}(\vec{x}, \omega) e^{j\omega t} \right] = \frac{1}{2} \left[\vec{E}(\vec{x}, \omega) e^{j\omega t} + \vec{E}^*(\vec{x}, \omega) e^{-j\omega t} \right], \quad (2.9)$$

where $\omega = 2\pi f$ represents the angular frequency, $j = \sqrt{-1}$, and $\Re[\cdot]$ denotes the real part. Inserting (2.9) into the wave equation (2.8) yields, since $\partial^2 \vec{E}(\vec{x}, \omega) / \partial \omega^2 = 0$, the HELMHOLTZ equation:

$$\nabla^2 \vec{E}(\vec{x}, \omega) + \frac{\omega^2}{c^2} \vec{E}(\vec{x}, \omega) = 0 \quad (2.10)$$

2.1 Plane Waves

The most simple solution for (2.10) is given by

$$\vec{E}(\vec{x}, \omega) = \vec{E}(\vec{k}, \omega) e^{-j\vec{k} \cdot \vec{x}}, \quad (2.11)$$

where \vec{k} is the wavevector. This expression can be directly inserted into (2.9) to get an equation for the electric field in the time domain,

$$\vec{\mathcal{E}}(\vec{x}, t) = \Re \left[\vec{E}(\vec{k}, \omega) e^{-j(\vec{k} \cdot \vec{x} - \omega t)} \right]. \quad (2.12)$$

The planes of constant phase for this solution of the HELMHOLTZ equation (2.10), $\vec{k} \cdot \vec{x} - \omega t = \text{const.}$, are orthogonal to the wavevector \vec{k} , so this solution is called plane wave. The wavenumber $k = |\vec{k}|$ can not be chosen independently of ω , the *dispersion relation* has to be met to let (2.12) solve (2.10):

$$k^2 = \frac{\omega^2}{c^2} \quad (2.13)$$

The physical meaning of k is that of a spatial frequency, e.g. two planes of constant phase are separated by the distance

$$\lambda = \frac{2\pi}{|\vec{k}|}, \quad (2.14)$$

which is called the wavelength. In vacuum, the wavelength is

$$\lambda_0 = \frac{2\pi}{k_0} = 2\pi \frac{c_0}{\omega} = \frac{c_0}{f}, \quad (2.15)$$

where $c_0 = 2.99792 \cdot 10^8$ m/s is the velocity of light in vacuum. One advantage of this type of wave is, besides its simplicity, the possibility to represent each other solution³ of the wave equation (2.8) by superposition (FOURIER-Integral). Applications where the use of plane waves is advantageous involve boundary value problems, like reflection and transmission calculations.

³Precisely, each valid solution that describes a propagating wave.

The Phase Velocity

Since plane waves, defined by (2.12), are propagating in space, a measure for the velocity of the surfaces of constant phase can be determined by differentiating the phase term:

$$\vec{k} \cdot \vec{x} - \omega t = \text{const.} \quad (2.16)$$

$$\vec{k} \cdot \frac{d\vec{x}}{dt} - \omega = 0 \quad (2.17)$$

Then, the *phase velocity* v_{ph} is given by

$$v_{ph} := \left| \frac{d\vec{x}}{dt} \right| = \frac{\omega}{k} = f\lambda, \quad (2.18)$$

which is comparable to the right hand side of (2.15) where $c_0 = v_{ph}$. From the Maxwell relation (2.7), the phase velocity can also be expressed in terms of ε and μ ,

$$v_{ph} = \frac{1}{\sqrt{\varepsilon\mu}} = \frac{1}{\sqrt{\varepsilon_0\mu_0}} \cdot \frac{1}{\sqrt{\varepsilon_r\mu_r}}, \quad (2.19)$$

where ε_r and μ_r denote the relative electric permittivity and the relative magnetic permeability, respectively. To be able to work with materials other than vacuum, it is useful to introduce the index of refraction⁴

$$n := \sqrt{\varepsilon_r\mu_r}. \quad (2.20)$$

The refractive index is, like the relative electric permittivity ε_r , also frequency-dependent. For vacuum, $n = 1$, and for air, n normally lies very close to 1. More detailed information on the index of refraction can be found in Section 3.1.

Using the index of refraction, the expression for the phase velocity v_{ph} (2.18) relative to vacuum (where $v_{ph} = c_0 = 1/\sqrt{\varepsilon_0\mu_0}$) becomes,

$$v_{ph} = \frac{c_0}{n} = f \frac{\lambda_0}{n}, \quad (2.21)$$

so the index of refraction changes the wavelength of the propagating wave. With this result, the HELMHOLTZ equation (2.10) can be rewritten in the form

$$\nabla^2 \vec{E}(\vec{x}, \omega) + k^2 n^2 \vec{E}(\vec{x}, \omega) = 0, \quad (2.22)$$

and the wave equation becomes

$$\nabla^2 \vec{\mathcal{E}}(\vec{x}, t) + k^2 n^2 \frac{\partial^2 \vec{\mathcal{E}}(\vec{x}, t)}{\partial t^2} = 0. \quad (2.23)$$

2.2 Spherical Waves

One big disadvantage of plane waves is that the location of their source is not defined. To solve this problem, another Ansatz has to be chosen:

$$\vec{\mathcal{E}}(\vec{x}, t) = u(\vec{x}) e^{-j(kz - \omega t)}, \quad (2.24)$$

⁴Setting $\mu_r = 1$ does not restrict the applications treated in this work.

where $u(\vec{x})$ is the location-dependent amplitude, and $k = k_z$ is the component of the wavevector \vec{k} in the z -direction. Inserting the amplitude of (2.24), $u(\vec{x}) \exp[-jkz]$, into the HELMHOLTZ Equation (2.22), and neglecting the time dependency, yields

$$\nabla^2 u(\vec{x}) + 2jk \frac{\partial u(\vec{x})}{\partial z} + k^2 n^2 u(\vec{x}) = 0. \quad (2.25)$$

Assuming that the amplitude u does not vary too much in the propagation direction (which is the z -axis in this case) along a distance λ , the so-called *slowly varying envelope* approximation,

$$\lambda \left| \frac{\partial^2 u(\vec{x})}{\partial z^2} \right| \ll 2\pi \left| \frac{\partial u(\vec{x})}{\partial z} \right|, \quad (2.26)$$

can be used to neglect the partial derivative in z in the Nabla-operator $\vec{\nabla}$, compared to the partial derivative in the second term of Eqn. (2.25), to get to another version of the HELMHOLTZ equation, called the *paraxial* HELMHOLTZ equation:

$$\nabla_T^2 u(\vec{x}) + 2jk \frac{\partial u(\vec{x})}{\partial z} + k^2 n^2 u(\vec{x}) = 0, \quad (2.27)$$

with $\nabla_T^2 = \partial^2/\partial x^2 + \partial^2/\partial y^2$. It can be verified that

$$u(\vec{x}) = \frac{u_0}{\vec{x}} e^{-jk|\vec{x}|} \quad (2.28)$$

solves the paraxial HELMHOLTZ equation. In this solution surfaces of constant phase are spheres, the center lying at $|\vec{x}| = 0$. As with the plane waves, the phase velocity v_{ph} is ω/k , and the distance, or difference in the radii, of two planes of constant phase is λ .

2.3 Gaussian Beam

The problem with the solutions of the wave equation mentioned before (plane wave (Sect. 2.1) and spherical wave (Sect. 2.2)) lies within their structure: As it is impossible to determine a dedicated point source in the case of a plane wave, the spherical wave's source is clearly defined. But a closer look at the divergence of those wave types reveals that the spherical wave has the largest possible, while that of a plane wave is zero.

Since the goal of this diploma thesis is to examine atmospheric effects on laser beams, these wavetypes are not satisfactory. Of course, one can approximate a laser beam by a plane wave when looking only at a small part of its illumination area in the far field, but my intention is to provide a solution that is as universal as possible. So, what has to be found is a combination of those two types, and the Gaussian beam profile is a good and relatively easy-to-handle mathematical construct that fulfills these needs – well defined divergence, source, and propagation direction.

The first step for the derivation of the formulas for the Gaussian beam is to switch from cartesian (x, y, z) to cylindric (r, ϕ, z) coordinates. A beam is characterized by the localization of the major part of its energy around the propagation direction, hence the following

approximation can be used:

$$\begin{aligned}
 |\vec{x}| &= \sqrt{x^2 + y^2 + z^2} \\
 &= \sqrt{r^2 + z^2} \\
 &= z\sqrt{1 + \frac{r^2}{z^2}} \\
 &\approx z + \frac{r^2}{2z}
 \end{aligned} \tag{2.29}$$

In the last step, I used the approximation $\sqrt{1+x} \approx 1+x/2$, applicable when $x^2 + y^2 \ll z^2$, which is assumed to be the case. The absolute value of the vector lying orthogonal to the propagation axis, $|\vec{x}_T|$, is $r = \sqrt{x^2 + y^2}$. Thus, (2.28) can be written as

$$\frac{u_0}{\vec{x}} e^{-jk|\vec{x}|} \approx \frac{u_0}{z} e^{-jkr^2/2z} e^{-jkz}. \tag{2.30}$$

Compared to (2.24), the amplitude function is

$$u(\vec{x}) = \frac{u_0}{z} e^{-jkr^2/2z}. \tag{2.31}$$

The Gaussian beam is a solution of the paraxial Helmholtz equation (2.27). The amplitude of the spherical wave (2.31) also solves (2.27), but with the disadvantage of a singularity at the center, $z = 0$. Substituting $z \rightarrow z + jz_0$, $z_0 = \text{const.}$, which corresponds to a shift in the complex plane, does not influence the validity of solution (2.24), but leads to many interesting properties. First of all, the singularity is moved out of the center of the complex plane. In the amplitude function (2.31),

$$u(\vec{x}) = \frac{u_0}{z + jz_0} \exp \left[-j \frac{kr^2}{2(z + jz_0)} \right], \tag{2.32}$$

the term $1/(z + jz_0)$ can be split up into the real and imaginary part [2],

$$\frac{1}{z + jz_0} = \frac{z - jz_0}{z^2 + z_0^2} =: \frac{1}{R} - j \frac{2}{kw^2(z)}, \tag{2.33}$$

with the parameters

$$R(z) = z \left[1 + \left(\frac{z_0}{z} \right)^2 \right] \tag{2.34}$$

$$w^2(z) = w_0^2 \left[1 + \left(\frac{z}{z_0} \right)^2 \right], \tag{2.35}$$

where

$$w_0^2 := 2z_0/k = \lambda z_0/\pi, \tag{2.36}$$

was is used (z_0 is also known as the confocal parameter). The importance of (2.34) and (2.35) will be made clear soon. Now, the amplitude function (2.32) can be written as follows:

$$u(\vec{x}) = u'_0 \frac{w_0}{w(z)} \exp \left[-\frac{r^2}{w^2(z)} \right] \exp \left[-jk \frac{r^2}{2R(z)} \right] e^{-j\xi(z)}, \tag{2.37}$$

$u'_0 := \frac{u_0}{jz_0}$, and $\xi(z) = \arctan\left(\frac{z}{z_0}\right)$ results from the representation of the complex amplitude $u'_0 jz_0/(z + jz_0)$ in polar coordinates.

The phase front curvature, given by the complex term $\exp[-jkr^2/2R(z)]$ in (2.37), depends on k , r , and $R(z)$, which stands for the radius of the phase front. This radius is determined by (2.34). The phase fronts are paraboloidal, thus comparable to spheres with the radius equal to the radius of curvature $R(z)$. At $z = 0$, the radius becomes $R = \infty$, and at $z = z_0$, the radius reaches its minimal value, until R becomes approximately as large as z for $z \gg z_0$.

The radius of the Gaussian beam after the propagation distance z is determined by (2.35). It depends on the initial beam waist radius, and on the confocal parameter z_0 . It is also possible to obtain the beam radius by calculating the standard deviation of (2.37). The standard deviation is the squareroot of the variance, which is defined by

$$\sigma_r^2 = \int_{-\infty}^{\infty} (r - \mu_{\vec{r}})^2 u(\vec{r}, z) d\vec{r}, \quad (2.38)$$

where $\mu_{\vec{r}}$ is the mean of $u(\vec{r}, z)$. In the following chapters, the Gaussian beam will be affected by random quantities, but by using (2.38), it will still be possible to calculate the beam radius at any distance.

Some properties of the Gaussian beam can be seen in Fig. 2.1, where the shape of a Gaussian beam (as seen normal to the propagation direction) with a confocal parameter z_0 and the resulting beam waist w_0 is plotted (note that at a given wavelength, only one of these two parameters can be chosen, cf. (2.34), (2.35), and (2.36)).

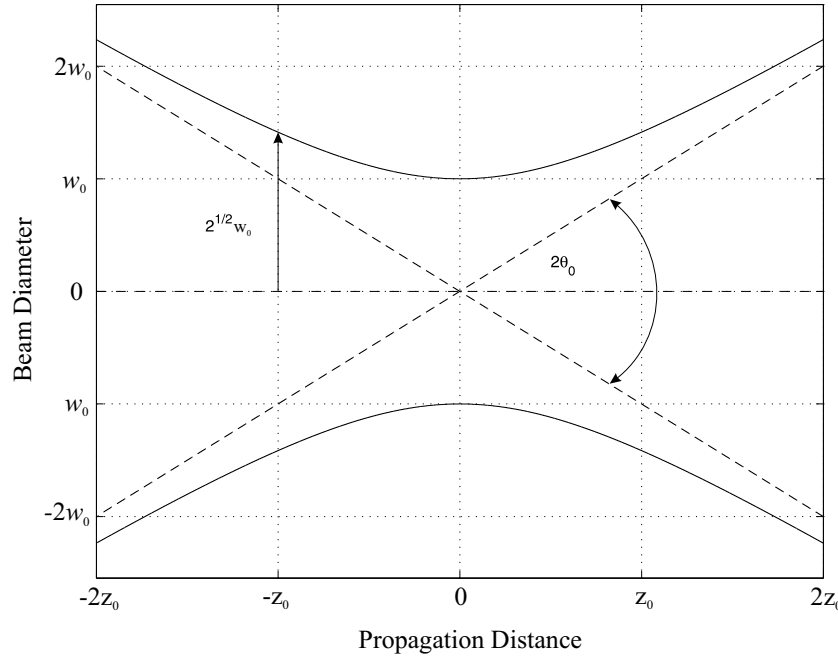


Figure 2.1: Transversal intensity profile of a Gaussian beam

The area where $|z|$ is less or equal z_0 is called 'confocal area', and it is common use to define the beam as being focused where $|z| < 2z_0$. When $|z|$ is larger than $2z_0$, the increase in

beam diameter, also called spreading or divergence, can be estimated from

$$2\theta_0 = 2 \arctan \frac{w_0}{z_0} \approx 2 \frac{w_0}{z_0} = \frac{2\lambda}{\pi w_0}, \quad (2.39)$$

where θ_0 is the divergence angle in radians.

In Chapter 5, the focus will be laid on the absolute value of the beam diameter $2w$ at a certain distance L from the transmitter. For vacuum, it suffices to multiply θ_0 with the propagation distance to get a measure for the spreading of the beam since the paraxial approximation can be used:

$$2w(L) = 2(w_0 + \theta_0 L) = 2 \left(w_0 + \frac{\lambda}{\pi w_0} L \right) \quad (2.40)$$

Here, the first term is needed for small propagation distances and for large beam diameters at the transmitter.

Chapter 3

Waves in Random Media

In this chapter, I will give an overview about different methods used throughout literature to solve problems related to wave propagation in random media, that is, with randomly changing index of refraction. I will start with the definition of the index of refraction n and its dependencies, followed by an introduction of the moments of the stochastic field. The main focus of this chapter will be laid on the different approaches that have been made to approximate solutions for the wave equation.

3.1 Index of Refraction

The physical meaning of the index of refraction n as a property of a medium is the ratio of the velocity of light in vacuum to the velocity of light in this medium. Since the frequency of a wave does not change its value, the wavelength depends on the environment (2.21). Figure 3.1

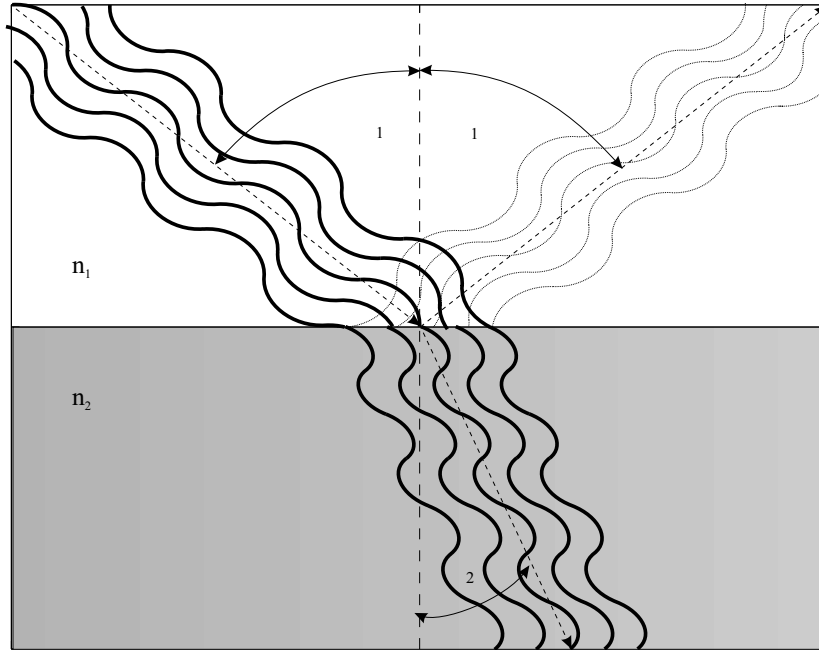


Figure 3.1: Refraction and reflection at the boundary of dielectric media

shows a light ray impinging on the border between two media with different indices of refraction n_1 and n_2 (in this case: $n_1 < n_2$). The ray is reflected and transmitted. The angle of the reflected ray is equal to that of the incident one (θ_1), but the angle of the transmitted ray (θ_2) differs, and that difference is due to the unequal indices of refraction. The dependency of the angle of the transmitted wave on the index of refraction was first found by Willebrord Snell and is therefore called “Snell’s law of refraction”,

$$n_1 \sin \theta_1 = n_2 \sin \theta_2. \quad (3.1)$$

Generally speaking, the value of the refractive index’s lower limit equals one for vacuum, increasing with the density of the materials (about 1.00002 to 1.00005 for air, or 1.5 for most types of glass). Since perfect homogeneous materials do not exist, small variations of n have to be expected. Most of the time they will be negligible, but for the topic presented in this thesis, I will show that, although extremely small, these variations have a certain impact on wave propagation.

Examples for the impact of air on the propagation of light can be observed in everyday’s life: Looking at the stars during a clear night, one does not see a settled picture, the stars appear to be twinkling (more precisely, they appear to change their light intensity). This phenomenon is a result of the atmosphere. Other well-known phenomena are the flicker of hot air, the appearance of a mirage, or ‘looming’ – one can see farther than the horizon at night. A mirage evolves when a hot layer of air near ground induces a decrease in air density, leading to a reduction of the refractive index. It can be seen directly from (3.1) that the emerging ray will bend upwards ($\theta_2 > \theta_1$) – towards the denser medium – and will leave the impression of a mirrored object on the observer’s eye.

The appearance of these phenomena can not be observed all the time, it is depending on the environment. Therefore, it can be found that an additive dispartment of the refractive index should be possible: First, there will be a constant term identical to undisturbed propagation in vacuum, $n_{\text{vac}} = 1$. The second term, n_{flc} , will represent the fluctuating effects, e.g. the twinkling, thus is random. An expression for the pressure and temperature dependent second term can be found in [1, 3, 4],

$$n = n_{\text{vac}} + n_{\text{flc}} \quad (3.2)$$

$$n_{\text{vac}} = 1 \quad (3.3)$$

$$n_{\text{flc}} = 77.6 \cdot 10^{-8} \left(1 + \frac{7.52 \cdot 10^{-15} \text{ m}^2}{\lambda^2} \right) \frac{p}{T} \frac{\text{ms}^2\text{K}}{\text{kg}}, \quad (3.4)$$

where p [Pa] stands for the local pressure, and T [K] is the local temperature. Comparing the properties of local pressure and those of local temperature, it suffices to observe only the temperature fluctuations. The pressure is depending on the temperature, and it can be shown that changes in the local temperature due to changes of the local pressure can be neglected [5].

With regard to further calculations, it is useful to separate the refractive index in another way than in (3.2),

$$n = n_0 + n_1, \quad (3.5)$$

where n_0 represents the mean of the refractive index, and n_1 is the mean-free, fluctuating part (n_{flc} in (3.4) is not mean-free).

As will be seen in the following sections, it is impossible to state an expression that exactly solves the wave equation with a random index of refraction. The necessity for stochastic models and methods will become clear.

3.2 Moments of the Field

The representation of a medium with randomly varying properties by a stochastic field becomes useful for further analysis. It is impossible to find exact predictions for one realization of the stochastic field, like the speed of wind at a determined time t_0 , or the amplitude of the electric component of a wave after passing through random inhomogeneities. Therefore, other parameters have to be introduced so that qualitative statements can be made. Examples are the *Moments of the Field*, generally defined by [3]

$$\begin{aligned}\Gamma_{m,n}(\vec{r}_1, \vec{r}_2, \dots, \vec{r}_m; \vec{r}'_1, \vec{r}'_2, \dots, \vec{r}'_n; z) &= \langle u(\vec{r}_1, z) \dots u(\vec{r}_m, z) u^*(\vec{r}'_1, z) \dots u^*(\vec{r}'_n, z) \rangle \\ &= \left\langle \prod_{i=1}^m u_i(\vec{r}_i; z) \prod_{j=1}^n u_j^*(\vec{r}'_j; z) \right\rangle.\end{aligned}\quad (3.6)$$

The sum of the indices m and n defines the order of the moment, e.g. the order of the moment $\Gamma_{1,0}$ is one, or that of the moment $\Gamma_{2,2}$ is four.

The vector \vec{r} is defined in the same way as in Sect. 2.3, $\vec{x} = \vec{r} + z\vec{e}_z$, i.e., it stands for the distance and direction of a vector that points from the middle of a plane (that lies perpendicular to the propagation direction) to an arbitrary point. The two vectors \vec{r}_i and \vec{r}'_i are independent.

One component of the field is given by $u(\vec{r}_k, z)$, e.g.¹

$$E(\vec{r}_k, z) = u(\vec{r}_k, z) \exp(jkz), \quad (3.7)$$

while $u^*(\vec{r}'_l, z)$ is the complex conjugate of $u(\vec{r}'_l, z)$.

The moment of first order, or *mean field*, is given by

$$\Gamma_{1,0}(\vec{r}, z) = \langle u(\vec{r}, z) \rangle. \quad (3.8)$$

It can be interpreted as the coherent part of the field.

The synonym *Mutual Coherence Function* (MCF) stands for the second order moment of the field,

$$\Gamma_{1,1}(\vec{r}_1; \vec{r}'_1; z) = \langle u(\vec{r}_1, z) u^*(\vec{r}'_1, z) \rangle. \quad (3.9)$$

The physical meaning of this expression is not obvious at the moment, but when both radii are set to the same value $\vec{\rho}$, the mean intensity $\bar{I}(\vec{P})$ at the point $\vec{P} = \vec{\rho} + \vec{z}$ is given by

$$\bar{I}(\vec{P}) = \Gamma_{1,1}(\vec{\rho}; \vec{\rho}; z). \quad (3.10)$$

Another interesting property of the stochastic field, deduced from the second order moment of the field, is the coherence length ρ_0 . It is defined by the distance where the absolute value of the *complex degree of coherence*,

$$\gamma(\vec{r}_1; \vec{r}'_1; z) = \frac{\Gamma_{1,1}(\vec{r}_1; \vec{r}'_1; z)}{\sqrt{\Gamma_{1,1}(\vec{r}_1; \vec{r}_1; z) \Gamma_{1,1}(\vec{r}'_1; \vec{r}'_1; z)}} \quad (3.11)$$

becomes equal to $\exp[-1]$. For locally homogeneous and isotropic fields, this reads

$$|\gamma(r = \rho_0)| = \exp[-1]. \quad (3.12)$$

¹The time dependency is assumed to be strictly harmonic, thus not mentioned here explicitly.

The complex degree of coherence lies within the interval $[0, 1]$; for plane waves (or for areas of other wavetypes that can be approximated by plane waves), γ is solely a function of the absolute value of $r = |\vec{r}_1 - \vec{r}'_1|$.

The fourth order moment of the field is

$$\Gamma_{2,2}(\vec{r}_1, \vec{r}_2; \vec{r}'_1, \vec{r}'_2; z) = \langle u(\vec{r}_1, z)u_2(\vec{r}_2, z)u_1^*(\vec{r}'_1, z)u_2^*(\vec{r}'_2, z) \rangle. \quad (3.13)$$

This moment brings most of the trouble with it, as will be seen later in this chapter. In the form $\Gamma_{2,2}(\vec{r}_1, \vec{r}_2; \vec{r}'_1, \vec{r}'_2; z)$, the fourth order moment is equal to the variance of the intensity of the field.

It has been shown that including moments other than second and fourth order is not reasonable for the calculations made within this diploma thesis [4, 6]. Besides, there do not exist any approximations for moments of orders higher than four.

3.3 Solutions for the Stochastic Wave Equation

The wave equation (2.27) can not be solved in a simple way when a random refractive index is involved. In that case, there exist methods to get terms that can be used to approximate the desired quantity.

The various methods differ mainly in their physical approach to the problem of solving the wave equation, resulting in differences for their ranges of validity. However, these ranges are not very strict. It is unclear at this point what method has to be favoured because some methods yield widely different results for one task, while for another, there is only little deviation. So the results for the particular problem, obtained by different methods, have to be compared and evaluated. Unfortunately, it is impossible to determine the 'correct' approximate solution (the one with the smallest error), because to do so, one would need an exact expression or at least measured values from an experiment. (Unfortunately, it is not possible to set up an experiment in any case.)

For most of the methods presented here, which are the most important and widely used ones, I will give a derivation of the mathematical results. The ranges of validity will also be defined, and evaluations will be given for the use of some approximations with regard to the next chapter. (That chapter is about wave propagation through atmospheric turbulence.)

3.3.1 Direct Solution Methods

For some fields of interest, it is possible to derive solutions for the moments of the field by directly analyzing the stochastic wave equation. The two methods presented here can be used for that task.

Parabolic Equation Method

The parabolic equation method (PEM) can theoretically be applied under all atmospheric conditions [3, 4]. Equations for the different moments of the field are established using the paraxial HELMHOLTZ equation (2.27)²,

$$\nabla_T^2 u(\vec{r}; z) + 2jk \frac{\partial u(\vec{r}; z)}{\partial z} + k^2 n^2(\vec{r}; z) u(\vec{r}; z) = 0. \quad (3.14)$$

²The HELMHOLTZ equation is also known as the *parabolic* wave equation because its form is that of a parabolic differential equation.

Based on this expression, the first order moment, or mean field, is a solution of [6]

$$\nabla_T^2 \langle \Gamma_{1,0}(\vec{r}; z) \rangle + 2jk \frac{\partial \langle \Gamma_{1,0}(\vec{r}; z) \rangle}{\partial z} + k^2 \langle n^2(\vec{r}; z) \Gamma_{1,0}(\vec{r}; z) \rangle = 0, \quad (3.15)$$

or

$$\nabla_T^2 \langle u(\vec{r}; z) \rangle + 2jk \frac{\partial \langle u(\vec{r}; z) \rangle}{\partial z} + k^2 \langle n^2(\vec{r}; z) u(\vec{r}; z) \rangle = 0. \quad (3.16)$$

The parabolic equation satisfied by the second order moment is [6]

$$\begin{aligned} (\nabla_{T1}^2 + \nabla_{T1'}^2) \Gamma_{1,1}(\vec{r}_1; \vec{r}'_1; z) + 2jk \frac{\partial}{\partial z} \Gamma_{1,1}(\vec{r}_1; \vec{r}'_1; z) + \\ + k^2 \langle [n_0^2(\vec{r}; z) - n_1^2(\vec{r}; z)] u(\vec{r}_1; z) u^*(\vec{r}'_1; z) \rangle = 0. \end{aligned} \quad (3.17)$$

An exact expression for the solution of this set of equations has been obtained only for the cases of plane and spherical waves. An analytic expression for the fourth order moment doesn't exist.

The PEM includes multiple forward scattering and ignores backscattering. It takes into account diffraction in the Fresnel approximation. Detailed information about this method can be found in [4].

Since the Gaussian beam is employed in further calculations, this method can not be used. In addition, the fourth order moment of the field is necessary to analyze some impacts on a laser beam; the parabolic equation method does not provide solutions for this particular moment.

Extended Huygens–Fresnel Principle

An approach to find a solution for the HELMHOLTZ equation (2.22) similar to the parabolic equation method was developed by Lutomirski and Yura in the United States (see [7] for a short description and further references), and by Feizulin and Kravtsov in the former USSR [6]. They used the Huygens–Fresnel integral,

$$u_0(\vec{r}; z) = -2jk \int_{-\infty}^{\infty} G(\vec{s}, \vec{r}; z) u_0(\vec{s}; 0) d\vec{s}, \quad (3.18)$$

where $G(\vec{s}, \vec{r}; z)$ is *Fresnel's approximation of Green's function*³

$$G(\vec{s}, \vec{r}; z) = \frac{1}{4\pi z} \exp \left[j \left(kz + \frac{k}{2z} |\vec{s} - \vec{r}|^2 \right) \right]. \quad (3.19)$$

The integral (3.18) is a solution of the wave equation for free-space propagation ($u_0(\vec{r}; z)$ stands for the vacuum solution). The necessary extension to solve the stochastic wave equation reads

$$u(\vec{r}; z) = -\frac{jk}{2\pi z} \exp(jkz) \int_{-\infty}^{\infty} u_0(\vec{s}; 0) \exp \left(\frac{jk|\vec{s} - \vec{r}|^2}{2z} + \psi(\vec{r}, \vec{s}) \right) d\vec{s}. \quad (3.20)$$

³Fresnel's approximation of Green's function can be used when $\lambda \ll l_0$, and $\lambda z / l_0^2 \ll (l_0 / \lambda)^2$, where l_0 is the smallest size of inhomogenities.

The field at the origin is given by $u_0(\vec{s}; 0)$, and $\psi(\vec{r}, \vec{s})$ is the random part of the complex phase of a spherical wave propagating in the turbulent medium from the point $(\vec{s}, 0)$ to the point (\vec{r}, z) .

As with the parabolic equation method, it has been shown that the extended Huygens–Fresnel principle is applicable under all atmospheric conditions, but there exist only solutions for the first and the second order field moments. For the fourth order field moment, (3.20) can be used only with certain restrictions [6].

Rytov *et al.* derived quite complicated expressions for the first and second order moment of the field [4]. As with the parabolic equation method, an expression for the fourth order moment of the field that is needed for further calculations can not be supplied. That is the reason why I did not further analyze this method.

3.3.2 Geometrical Optics Method

Geometrical optics refer to ray tracing methods. The starting point are plane TEM (Transversal–Electro–Magnetic) waves (like those described in Sect. 2.1), with the propagation direction being normal to the phase fronts (= “rays”). These rays will travel in straight lines in a homogeneous medium, and when this medium changes its refractive index, they obey Snell’s law. Effects of total reflection can also be described. The geometrical optics method can be used to analyze spherical waves.

Since this approach uses the model of (incoherent) light rays, it is incapable of describing effects like diffraction or interference. These effects arise from the light’s nature of being a wave. But within its scope, the geometrical optics method (GOM) has definite advantages over some other methods. It is easily possible to describe, e.g., the influence of regular refraction, or large field fluctuations [4].

The use of the GOM with atmospheric turbulence is justified if the following conditions are fulfilled:

- The smallest scale of turbulence is much larger than the wavelength, $l_0 \gg \lambda$. The *inner scale of turbulence*, l_0 , will be discussed in detail in the next chapter. Measurements have shown that the typical inner scale size varies from 5 mm to 12 mm, so for optical frequencies, this condition will always be met [8].
- The first Fresnel zone has to be much smaller than a typical minimum scale size of the turbulence, $\sqrt{\lambda L} \ll l_0$, where L is the propagation distance. Inserting $l_0 = 8$ mm and $\lambda = 1.55 \mu\text{m}$ shows the shortcoming of this method, it restricts the length of the propagation path to a maximum of a few tens of meters.

This method seems to be incapable of deriving results needed for calculations in the field of Earth–Satellite laser communication systems. Nevertheless, it has to be outlined that for longer pathlengths, the geometrical optics solution for phase (not amplitude) fluctuations lies within the order of the results obtained by other approximations. This fact and the simplicity of the GOM are the main reasons why this method is used in various astronomical applications and in adaptive optics development.

The GOM is not treated in detail here because both phase and amplitude fluctuations are needed when an optical communication system is analyzed. An extensive description can be found in [4].

3.3.3 Born Approximation

The purpose of the methods presented in subsection 3.3.1 is to find equations for the moments of the field by directly solving the wave equation. I pointed out the restrictions, namely that solutions for the Gaussian beam and for the fourth order moment of the field do not exist.

Another way for deriving expressions for the moments is by applying perturbation methods to different equations, in case of the Born approximation (or method of small perturbations, MSP), to the HELMHOLTZ equation (2.22). The goal of this method is to separate the random coefficient n from the quantity for which one wishes to solve u , so out of (2.22) (omitting the z -dependency),

$$\nabla^2 u(\vec{r}) + k^2 n^2 u(\vec{r}) = 0, \quad (3.21)$$

one wants to get an expression of the form

$$\nabla^2 u(\vec{r}) + k^2 u(\vec{r}) = f(\vec{r}), \quad (3.22)$$

where the random refractive index appears as a factor in $f(\vec{r})$.

The index of refraction $n(\vec{r}, z)$ is expanded into a series⁴ (3.5),

$$\begin{aligned} n^2(\vec{r}, z) &= [1 + n_1(\vec{r}, z)]^2 \\ &\approx 1 + 2n_1(\vec{r}, z), \quad |n_1(\vec{r}, z)| \ll 1, \end{aligned} \quad (3.23)$$

The first part of (3.5) is constant, and the mean-free fluctuating part is a small random quantity; thus, n_1^2 is much smaller than n_1 and can be neglected. The next step is to expand the components of the optical field $u(\vec{r}, z)$ into a series,

$$u(\vec{r}, z) = u_0(\vec{r}, z) + u_1(\vec{r}, z) + u_2(\vec{r}, z) + \dots, \quad (3.24)$$

where the contributions $|u_i|$ strongly decrease in magnitude with increasing order i . The symbol $|u_0|$ denotes the absolute value of the unperturbed portion of the field, and the other terms represent higher order perturbation terms, caused by the random inhomogeneities. Inserting (3.24) and (3.23) into (3.21) and separating the equations after the order of the perturbation yields

$$\nabla^2 u_0 + k^2 u_0 = 0 \quad (3.25)$$

$$\nabla^2 u_1 + k^2 u_1 = -2k^2 n_1 u_0 \quad (3.26)$$

$$\nabla^2 u_2 + k^2 u_2 = -2k^2 n_1 u_1 \quad (3.27)$$

...

To solve these equations, one can make use of Fresnel's approximation of Green's function (3.19) in cylindrical coordinates (inserting $z - L$ for z , where L is the overall propagation distance) to arrive at a solution for u_1 in an integral form [3, 6],

$$u_1(\vec{r}, L) = \frac{k^2}{2\pi} \int_0^L \int_{-\infty}^{\infty} \exp \left[j \left(k(L - z) + \frac{k|\vec{s} - \vec{r}|^2}{2(L - z)} \right) \right] u_0(\vec{s}, z) \frac{n_1(\vec{s}, z)}{L - z} d\vec{s} dz, \quad (3.28)$$

which is known as the *first Born approximation*. The physical interpretation is given by the association that the field perturbation u_1 is a sum of spherical waves with different magnitudes

⁴The squared index of refraction, n^2 , is examined since this is needed in (2.22).

that are proportional to the product of the initial field $u_0(\vec{s})$ and the local index of refraction $n_1(\vec{s})$. Since, by definition, $\langle n_1(\vec{s}, z) \rangle = 0$, it follows that the ensemble average of the first order Born approximation is zero as well, $\langle u_1(\vec{r}, L) \rangle = 0$.

To solve for the higher order terms, the similarity between (3.26) and (3.27) reveals that these equations are almost the same (the only difference lies within the index of the field, u_i). Thus, the solutions for these equations will resemble (3.28),

$$u_m(\vec{r}, L) = \frac{k^2}{2\pi} \int_0^L \int_{-\infty}^{\infty} \exp \left[j \left(k(L-z) + \frac{k|\vec{s} - \vec{r}|^2}{2(L-z)} \right) \right] u_{m-1}(\vec{s}, z) \frac{n_1(\vec{s}, z)}{L-z} d\vec{s} dz, \quad (3.29)$$

where $m = 1, 2, 3, \dots$. The inner integral has to be computed over the vector $d\vec{s}$ that lies in the plane orthogonal to the propagation direction, and the outer intergral has to be carried out over the propagation path. It has been shown that perturbation terms of orders higher than $m = 2$ are not important [4]. Note that, in general, $\langle u_m \rangle \neq 0$. In the next section, I will show that the Rytov and the Born approximation are very similar, and the expressions for the moments of the field that will be derived at the end are valid for both approximation methods.

The range of validity of the Born approximation is determined by the comparison of the unperturbed field with the perturbed field, $|u_0| \gg |u_1|$. This condition normally applies to weakly inhomogenous environments (the mathematical distinction when environments can be classified as weak or strong can be found in Sect. 4.5).

3.3.4 Rytov Approximation

The Rytov approximation (western notation), or method of smooth perturbations (MSP, former USSR), was introduced by Obukhov, who used a method suggested by Rytov. Like the Born approximation, the Rytov approximation is much more versatile than the GOM because it takes diffraction effects into account to a certain degree. Compared to the Born approximation, the computational effort remains the same. The intention for the introduction of the Rytov approximation was the extension of the range of validity of the Born approximation. However, it has been shown that the Born approximation can be mathematically transferred to the Rytov approximation, and that the range of validity will therefore be the same.

In his original work, Rytov applied his method to the parabolic wave equation (2.27), while Obukhov used the HELMHOLTZ equation (2.22) as the starting point [1, 3, 9]. In this work, I will refer to the method suggested by Obukhov.

The Rytov method uses the logarithm of the field instead of the field itself to approximate solutions for the wave equation. This is done by choosing

$$u(\vec{r}, z) = \exp[\Phi(\vec{r}, z)] \quad (3.30)$$

for one part of the electric field, where $\Phi(\vec{r}, z)$ is an auxiliary variable. As before, the electric field is given by

$$E(\vec{r}, z) = u(\vec{r}, z) \exp(jkz). \quad (3.31)$$

With this Ansatz, the HELMHOLTZ equation (2.27) is transformed to the nonlinear Riccati equation [1, 3],

$$\nabla^2 \Phi(\vec{r}, z) + [\vec{\nabla} \Phi(\vec{r}, z)]^2 + k^2 n^2(\vec{r}, z) = 0. \quad (3.32)$$

This equation has the advantage that the random coefficient n enters in an additive manner, not as a multiplicative factor.

In the previous subsections, the electrical field was decomposed by its order, now leading to a decomposition of the exponential term $\Phi(\vec{r}, z)$ (cf. (3.30) and (3.24)),

$$\Phi(\vec{r}, z) = \Phi_0(\vec{r}, z) + \Phi_1(\vec{r}, z) + \dots \quad (3.33)$$

Together with the additive dispartment of the refractive index (3.23), (3.33) is inserted into (3.32),

$$\nabla^2 [\Phi_0(\vec{r}, z) + \Phi_1(\vec{r}, z) + \dots] + \left\{ \vec{\nabla} [\Phi_0(\vec{r}, z) + \Phi_1(\vec{r}, z) + \dots] \right\}^2 + k^2 [1 + n_1(\vec{r}, z)]^2 = 0. \quad (3.34)$$

The next step to get to results for the moments of the field is to split the terms of (3.34) after their order [1],

$$\nabla^2 \Phi_0(\vec{r}, z) + [\vec{\nabla} \Phi_0(\vec{r}, z)]^2 + k^2 = 0 \quad (3.35)$$

$$\nabla^2 \Phi_1(\vec{r}, z) + 2\vec{\nabla} \Phi_0(\vec{r}, z) \cdot \vec{\nabla} \Phi_1(\vec{r}, z) + 2k^2 n_1(\vec{r}, z) = 0 \quad (3.36)$$

$$\nabla^2 \Phi_2(\vec{r}, z) + 2\vec{\nabla} \Phi_0(\vec{r}, z) \cdot \vec{\nabla} \Phi_2(\vec{r}, z) + k^2 n_1^2(\vec{r}, z) + \vec{\nabla} \Phi_1(\vec{r}, z) \cdot \vec{\nabla} \Phi_1(\vec{r}, z) = 0 \quad (3.37)$$

⋮

Similar to the Born approximation, it suffices to retain only the first three terms $\Phi_0(\vec{r}, z)$, $\Phi_1(\vec{r}, z)$, and $\Phi_2(\vec{r}, z)$, that are the unperturbed and the first and second order perturbed field, respectively. A physical interpretation of these three terms is given by the unperturbed part, and the single and double scattered parts of the wave. The equation for the unperturbed field (3.35) equals the common HELMHOLTZ equation (2.22). Expressing the lowest-order term in the form

$$u_0(\vec{r}, z) = \exp[\Phi_0(\vec{r}, z)], \quad (3.38)$$

which represents the solution of the wave equation for free-space propagation, (3.30) becomes

$$u(\vec{r}, z) = u_0(\vec{r}, z) \exp[\Phi_1(\vec{r}, z)] \exp[\Phi_2(\vec{r}, z)]. \quad (3.39)$$

To get a solution for the first order perturbation term $\Phi_1(\vec{r}, z)$, it is expressed as a weighted function of the unperturbed field,

$$\Phi_1(\vec{r}, z) = W_1(\vec{r}, z)/u_0(\vec{r}, z), \quad (3.40)$$

where $W_1(\vec{r}, z)$ is an auxiliary variable. Inserting this expression for $\Phi_1(\vec{r}, z)$ into (3.36) yields

$$\nabla^2 W_1(\vec{r}, z) + k^2 W_1(\vec{r}, z) + 2k^2 n_1^2(\vec{r}, z) u_0(\vec{r}, z) = 0. \quad (3.41)$$

This linear differential equation with constant coefficients can be solved using *Green's function*,

$$G(\vec{x} - \vec{x}') = \frac{1}{4\pi|\vec{x} - \vec{x}'|} \exp(jk|\vec{x} - \vec{x}'|), \quad (3.42)$$

yielding [1, 3]

$$\Phi_1(\vec{r}, z) = \frac{2k^2}{u_0(\vec{r}, z)} \int_V u_0(\vec{r}', z') n_1(\vec{r}', z') G(|\vec{r} - \vec{r}', z'|) dV', \quad (3.43)$$

where the integral has to be carried out over the volume \mathcal{V} (corresponding to the integration variables \vec{r}' and z'). Obtaining expressions for $\Phi_2(\vec{r}, z)$ in that way is rather difficult, but there exist other ways of deriving a solution.

Another method of deriving solutions for the stochastic wave equation is to extend the equations from the Born approximation [6]. To do so, I first introduce the *normalized* Born approximations,

$$\Psi_m(\vec{r}, z) = \frac{u_m(\vec{r}, z)}{u_0(\vec{r}, z)}, \quad m = 1, 2, 3, \dots, \quad (3.44)$$

with $u_m(\vec{r}, z)$ defined by (3.29). By setting equal the Rytov and Born approximations of first order (using $u_1(\vec{r}, z) = u_0(\vec{r}, z)\Psi_1(\vec{r}, z)$ for the first perturbation term of the Born approximation),

$$u_0(\vec{r}, z) \exp[\Phi_1(\vec{r}, z)] = u_0(\vec{r}, z) + u_1(\vec{r}, z) \quad (3.45)$$

$$= u_0(\vec{r}, z) (1 + \Psi_1(\vec{r}, z)) \quad (3.46)$$

it is found, upon dividing by $u_0(\vec{r}, z)$ and taking the natural logarithm, that both approximations are approximately equal,

$$\Phi_1(\vec{r}, z) = \ln(1 + \Psi_1(\vec{r}, z)) \quad (3.47)$$

$$\approx \Psi_1(\vec{r}, z), \quad |\Psi_1(\vec{r}, z)| \ll 1. \quad (3.48)$$

For the second order approximation, this method leads to [6]

$$\Phi_2(\vec{r}, z) = \Psi_2(\vec{r}, z) - \frac{1}{2}\Psi_1^2(\vec{r}, z), \quad |\Psi_1(\vec{r}, z)|, |\Psi_2(\vec{r}, z)| \ll 1. \quad (3.49)$$

It has been found that it is necessary to include perturbation terms of the order of two to keep the error of the approximation small [3, 4]. The zeroth and first order perturbation terms are sufficient for deriving results for the log-amplitude variance, the phase variance, intensity and phase correlation functions, and wave structure functions.

But to calculate various impacts on a laser beam, higher order statistical moments of the field are needed, thus it is necessary to incorporate the second order perturbation term in addition to the perturbation term of first order.

Since we have expressions for the (random) field components at hand now, the moments of the field can be determined. For example, to get the first order moment of the field, one has to insert

$$u(\vec{r}, z) = \exp[\Phi(\vec{r}, z)] = \exp[\Phi_0(\vec{r}, z) + \Phi_1(\vec{r}, z) + \Phi_2(\vec{r}, z) + \dots], \quad (3.50)$$

into (3.8) to get

$$\begin{aligned} \Gamma_{1,0}(\vec{r}, z) &= \langle u(\vec{r}, z) \rangle \\ &= \langle \exp[\Phi_0(\vec{r}, z) + \Phi_1(\vec{r}, z) + \Phi_2(\vec{r}, z) + \dots] \rangle. \end{aligned} \quad (3.51)$$

To be able to transform the ensemble average into the exponent, the method of cumulants is involved [6],

$$\langle \exp[\alpha] \rangle = \lim_{t \rightarrow -j} \langle \exp[jt\alpha] \rangle \quad (3.52)$$

$$= \exp \left[K_1 + \frac{1}{2}K_2 + \frac{1}{6}K_3 + \dots \right], \quad (3.53)$$

where only the terms up to the second order will be used. The coefficients K are defined by

$$K_1 = \langle \alpha \rangle \quad (3.54)$$

$$K_2 = \langle \alpha^2 \rangle - \langle \alpha \rangle^2. \quad (3.55)$$

With this method, it is possible to simplify equation (3.51) to get (in terms of the normalized Born approximation),

$$\Gamma_{1,0}(\vec{r}, z) = u_0(\vec{r}, z) \left\langle \exp[\Psi_1(\vec{r}, z)] \exp\left[\Psi_2(\vec{r}, z) + \frac{1}{2}\Psi_1^2(\vec{r}, z)\right] \right\rangle \quad (3.56)$$

$$= u_0(\vec{r}, z) \exp\left[\langle \Psi_2(\vec{r}, z) \rangle + \frac{1}{2}\langle \Psi_1^2(\vec{r}, z) \rangle\right], \quad (3.57)$$

where $\exp[\Phi_0(\vec{r}, z)]$ is the initial field $u_0(\vec{r}, z)$, and, by definition, $\langle \Phi_1(\vec{r}, z) \rangle = \langle \Psi_1(\vec{r}, z) \rangle = 0$. Perturbation terms of orders higher than two are assumed to be negligible.

The second order moment of the field turns out to be [6]

$$\begin{aligned} \Gamma_{1,1}(\vec{r}_1; \vec{r}'_1; z) &= \langle u(\vec{r}_1, z) u^*(\vec{r}'_1, z) \rangle \\ &= u_0(\vec{r}_1, z) u_0^*(\vec{r}'_1, z) \langle \exp[\Phi(\vec{r}_1, z) + \Phi^*(\vec{r}'_1, z)] \rangle \\ &= u_0(\vec{r}_1, z) u_0^*(\vec{r}'_1, z) \exp[2 \cdot \langle \Psi_2(\vec{r}_1, z) \rangle + \\ &\quad + \langle \Psi_1(\vec{r}_1, z) \rangle + \langle \Psi_1(\vec{r}_1, z) \Psi_1^*(\vec{r}'_1, z) \rangle]. \end{aligned} \quad (3.58)$$

Exact expressions for the fourth order moment do not exist. This particular moment would be needed for some calculations in Chapt. 5, but it is also possible to approximate results using other methods.

The range of validity of the Rytov approximation is determined by $|\vec{\nabla} \Phi_{n+1}(\vec{r}, z)| \ll |\vec{\nabla} \Phi_n(\vec{r}, z)|$, otherwise, the series (3.33) would converge too slowly.

The Rytov approximation is one of two methods that seems to predict the influence of the atmosphere for ground to space communication (and vice versa) with sufficient accuracy. Many authors derived equations for various effects (e.g., [1, 3, 6]), and measurements seem to confirm the results obtained by the Rytov method [9]. Nevertheless, ongoing discussions lead to doubts about the correctness of the application of this method. An alternative method is given by the Markov approximation.

3.3.5 Markov Approximation

A major restriction of the Born approximation and the Rytov approximation is their applicability to propagation paths where the influences on the wave can be classified as strong (since the specifications for the propagation path still have to be checked, this scenario must not be disregarded). The Markov approximation overcomes this restriction, while still being applicable within environments where the fluctuations are small. Like all the other methods mentioned, this approximation does not take backscattering into account.

The Markov approximation leads to solutions for the moments of the field of first and second order, and the fourth order moment can be approximated [9]. These moments are calculated starting with the paraxial Helmholtz equation (2.27),

$$\nabla_T^2 u(\vec{r}; z) + 2jk \frac{\partial u(\vec{r}; z)}{\partial z} + k^2 n^2(\vec{r}; z) u(\vec{r}; z) = 0, \quad (3.59)$$

which can be used for calculations involving light beams with narrow angular spread, which is assumed to be the case.

The difference between the Markov approximation and any other approximation presented in this work is that the fluctuating part of the index of refraction, $n_1(\vec{r}, z)$, is expected to be delta-function correlated in the propagation direction [4],

$$\langle n_1(\vec{r}, z) n_1(\vec{r}', z') \rangle = \delta(z - z') A(\vec{r} - \vec{r}', z) \quad (3.60)$$

with the delta-distribution given by

$$\delta(x - y) =: \begin{cases} 1 & \text{for } x = y \\ 0 & \text{else.} \end{cases} \quad (3.61)$$

In (3.60), the refractive index's dependency on the vector $(\vec{r} - \vec{r}')$ is given by

$$A(\vec{r} - \vec{r}', z) =: 8\pi \int_{-\infty}^{\infty} \Phi_n(\kappa_r, z) e^{j\vec{\kappa}_r \cdot (\vec{r} - \vec{r}')} d\vec{\kappa}_r. \quad (3.62)$$

The height-dependent spectrum of the index of refraction fluctuations $\Phi_n(\kappa_r, z)$ will be explained in detail in Sect. 4.4. The meaning of κ_r is comparable to a spatial frequency like the wavenumber k ; in this case, κ_r stands for the component orthogonal to the propagation direction. Section 4.4 contains more information about κ , like its exact definition.

The paraxial wave equation (3.59) can be solved for the moments of the field by using (3.60) along with the Novikov–Furutsu formula [3]. This formula provides a solution for the ensemble average of n_1 and u (that arises from (3.59)) if n_1 is a Gaussian random variable. The assumption that the refractive index's statistical distribution is Gaussian comes directly from the central limit theorem.

Ensemble averaging (3.59), inserting (3.60), and using the Novikov–Furutsu formula yields an equation for the first order moment of the field,

$$\nabla_T^2 \langle u(\vec{r}; z) \rangle + 2jk \frac{\partial \langle u(\vec{r}; z) \rangle}{\partial z} + \frac{jk^3}{4} A(\vec{r}, 0) \langle u(\vec{r}, z) \rangle = 0. \quad (3.63)$$

Prokhorov *et al.* [10] derived the same equation (3.63) from a more physical point of view, while Rytov *et al.* [4] derived this equation in a mathematically very strict way. Fante [9] solved this equation, leading to

$$\begin{aligned} \langle u(\vec{r}, z) \rangle &= - \left(\frac{jk}{2\pi z} \right) \int_{-\infty}^{\infty} u(\vec{r}', 0) \cdot \\ &\quad \cdot \exp \left[j \frac{k(\vec{r} - \vec{r}')^2}{2z} - \frac{k}{8} \int_0^z A(h, 0) dh \right] d\vec{r}' \end{aligned} \quad (3.64)$$

Strohben [3] found a much simpler solution for (3.63),

$$\langle u(\vec{r}, z) \rangle = \Gamma_{1,0}(\vec{r}; z) = u_0(\vec{r}, z) \exp \left[- \frac{k^2 A(z, 0) z}{2} \right], \quad (3.65)$$

where $u_0(\vec{r}, z)$ is the undisturbed wave. Although both solutions look different, they lead to the result that the mean field vanishes after a very short propagation distance. Therefore the first order moment of the field will be neglected in the calculations to follow.

For the second order moment of the field [3],

$$\left(2jk\frac{\partial}{\partial z} + \nabla_T^2 - \nabla_{T'}^2 + \frac{jk^3}{2}[A(0, z) - A(\vec{r} - \vec{r}', z)]\right) \Gamma_{1,1}(\vec{r}, \vec{r}'; z) = 0 \quad (3.66)$$

has to be solved (The indices of the nabla operator, T, T' , refer to the different radii, \vec{r} and \vec{r}'). A solution for (3.66) was found by Fante [9] and by Ishimaru (in [3]), but neither could I carry out the derivation nor could I verify these results.

The equation to solve for the fourth order moment of the field can be found in [3, 9], but analytic solutions do not exist. When needed, approximations will be introduced. They can be found in [3, 4, 9, 11].

Chapter 4

Laser Beam Propagation in the Atmosphere

For any free-space optical communication system, the atmosphere is the medium where the main part of the propagation of the laser beam takes place. This medium is special in the sense of attenuating and changing the properties of the laser beam. Attenuation results from the chemical elements of the atmosphere, mainly water vapor. This topic is briefly mentioned in Sect. 5.1 and Sect. 5.2, but for the remaining calculations, it is neglected. Another disregarded effect of the interaction between the atmosphere and a laser beam is the change of the atmospheric temperature and structure due to the power of the laser beam. This effect is called *Thermal Blooming*. More about it can be found in [3].

The structure of the atmosphere changes the properties of the laser beam passing through it. In this chapter, this structure is physically and mathematically described.

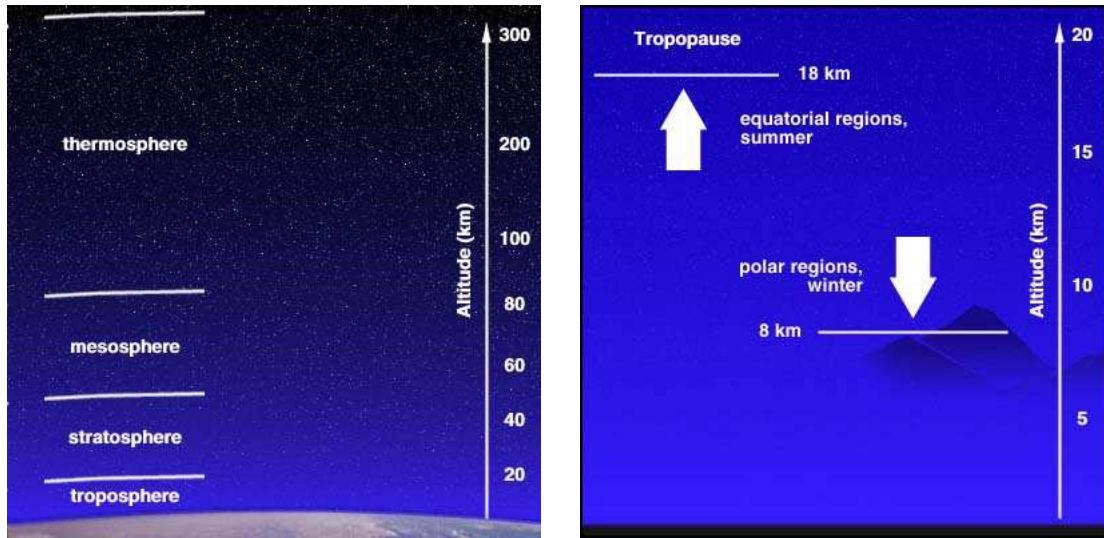
In the first section, I will present the topology and the contents of the atmosphere. Section 4.2 focuses on the definition and evolution of turbulence, and a section about structure functions that are used for describing random fields follows (Section 4.3). An introduction of the spectrum of turbulence that is needed to compute some moments of the field (see Sect. 3.2) will finalize this chapter.

4.1 Topology of the Atmosphere

The atmosphere¹ is the gaseous area surrounding the earth. Its density distribution is descending approximately exponentially with increasing height. The structure of the atmosphere can be split up into different layers lying parallel to the ground, but with varying borders (see Fig. 4.1(b)). Between these layers lie narrow transition zones. The upper limit at which gases disperse into space is situated at an altitude of approximately 1000 km, but more than 99% of the total atmospheric mass is concentrated in the first 40 km next to the earth's surface.

The atmosphere is a mixture of different types of gases and gaseous elements. A detailed decomposition and explanation of some chemical substances of content can be found in [13]. Besides gases like nitrogen, oxygen, carbon dioxide, and hydrogen, the atmosphere also contains water vapor and particulate material (also known as *aerosol*). The concentration of water vapor is strongly varying in time and space, but it is decreasing with increasing height due to the falling temperature. Dust, smoke, and small particles can be classified as 'particu-

¹greek: *atmos* = haze; *sphaira* = sphere



(a) Atmospheric layers

(b) The upper boundary of the troposphere.

Figure 4.1: Visualizations of the topology of the atmosphere (from [12]).

late material’, and one can distinguish between consolidated, gaseous, anorganic, and organic particles and microorganisms.

Since different elements of the atmosphere have different mass, one could expect that the lighter parts will be found at higher altitudes, while the parts with more mass reside next to the ground. But counterintuitively, the mixing ratio remains almost unchanged within distinct layers. This mixing is due to vertical turbulences. Horizontal turbulences are the reason why, e.g., the density of Oxygen (O_2) is the same above areas with high photosynthetic activity, like the tropics, and above regions where one would not expect it, like regions with a high density of industrial facilities [13].

Following Fig. 4.1(a), the atmosphere’s layers are (starting from ground and increasing altitude): the troposphere, the stratosphere, the mesosphere, the thermosphere, and the exosphere (not shown).

Troposphere: This atmospheric layer lies closest to the planet’s surface and contains the largest percentage of mass of the total atmosphere. The upper boundary is dependent on location and season: the troposphere ranges from 8 km in high latitudes to 18 km above the equator. Its expansion is largest in summer and lowest in winter (see Fig. 4.1(b)).

Depending on the season, the average temperature near ground varies from -30°C to 40°C . The average vertical change of temperature in the troposphere is approximately four degrees Celsius per kilometer, resulting in an average temperature of -60°C to -80°C at the upper bound. The amount of water vapor drops off quickly with increasing height². About 99% of the water vapor in the atmosphere is contained in the troposphere.

²Water vapor plays a major role in regulating the air temperature since it absorbs solar energy from the sun and thermal radiation from the planet’s surface.

The distribution of water vapor is location-dependent (about 3% to 4% above the tropics, decreasing towards the polar regions).

The troposphere is the layer where all weather phenomena occur (extensions into the lower stratosphere are possible). The troposphere can also be named the “region of mixing”, and this name comes from the strong convective air currents within this layer. A narrow zone called **Tropopause**, where air temperature remains constant, separates the troposphere from the next layer, the stratosphere.

Stratosphere: This layer resides between 10 and 50 km above the earth. Up to an altitude of about 25 km, the temperature remains approximately unchanged (at an average of -50°C), then it increases gradually to a range between -10°C and 0°C at the lower boundary of the stratopause layer. From then on, the temperature decreases again with increasing height. The increase of air temperature in the stratosphere results in a stabilization of atmospheric conditions in this region. The “most prominent” part of the stratosphere is the ozone layer at an altitude of 20 to 30 km; ozone overtakes the role of water vapor in this region, i.e., it regulates the temperature.

Mesosphere: Above the stratosphere, the mesosphere extends from approximately 50 km to 80 km; its lowest temperatures are in the range of -80°C to -90°C at highest altitudes. The concentrations of water vapor or ozone are negligible, leading to lower temperatures than in the lower layers. With an increase of distance from the earth’s surface, the chemical composition of the atmosphere becomes strongly altitude-dependent. At very high altitudes, the residual gases begin to stratify according to molecular mass, because of gravitational separation.

The **Mesopause Transition Layer** separates the Mesosphere from the Thermosphere.

Thermosphere: This part of the atmosphere reaches from approximately 80 km to 500 km. Temperatures are lower than in the mesosphere. At an altitude of 100 – 200 km, the major atmospheric components are still nitrogen and oxygen.

The Exosphere: This is the outermost region of the Earth’s atmosphere. The Exosphere begins at approximately 500 km and extends outwards to roughly 10000 km until it fades to interplanetary space. Atoms follow ballistic trajectories and rarely collide because the density of atoms in this region is low.

4.2 Turbulence

The atmosphere is in permanent motion. This motion arises as a consequence of a pressure gradient between a high-pressure and a low-pressure area (*anicyclone* and *cyclone* in meteorological terms, respectively). The atmosphere has the tendency to balance this difference in pressure. Air flows from the high-pressure area to the low-pressure area (*wind*). At the lowest 1500 m, the friction of the earth’s surface must not be neglected. This friction leads to a *turbulent* air flow.

The evolution of turbulence is made visible by an experiment [5]:

Consider an unlimited volume containing a fluid in motion. The direction of the motion is parallel to the x -direction in the xy -plane only. No boundaries are assumed, so the velocity vectors are strictly parallel. To find out how this fluid reacts when it is disturbed, a cylinder with infinite length, but a defined diameter l [m] is inserted into the flow. The cylinder’s

principal axis coincides with the z -axis. Next, the fluid needs to be specified by the absolute value of its characteristic velocity vector $|\vec{v}|$ [m/s] and its kinematic viscosity ν [m²/s]. Based on this values, it is possible to calculate the *Reynoldsnnumber* to classify the behaviour of the fluid,

$$Re =: \frac{|\vec{v}| \cdot l}{\nu}. \quad (4.1)$$

$Re \leq 10$: The flow will be strictly laminated, a slight loss of symmetry in the xy -plane is possible. The fluid can be described by deterministic means.

$10 \leq Re \leq \sim 40$: Some parts of the flow will start to mix and form “eddyies” (the vector of the velocity changes its direction clockwise or counterclockwise in these areas). At low Reynoldsnnumbers, a periodicity of those eddies establishes in the direction of the flow (*Kármánsche Wirbelstrasse* [14]). With increasing Re , the periodicity is lost, and the xy -plane is dominated by eddies.

$\sim 40 \dots 75 \leq Re$: At a certain Reynoldsnnumber that lies in this range, the symmetries in the xz -plane and in the yz -plane are also lost. In that case, the flow is seen as highly turbulent. Since the vectors of velocity point to various directions, only a stochastic approach can be used to describe the behaviour of the fluid.

In the atmosphere, the mixture of gases and small particles is similar to a fluid. A typical value for the kinematic viscosity of the atmosphere near ground is $\nu \in [10^{-4} \dots 10^{-6}]$ m²/s, decreasing with height³. Assuming low windspeeds, $|\vec{v}| \approx 1 \dots 5$ m/s and minimum typical dimensions of the disturbing elements on the order of a few millimeters, the lower bound for the Reynoldsnnumber near ground is on the order of approximately 500. With this value in mind, the atmosphere has to be considered highly turbulent, at least in the lowest layer, the troposphere, where the density has its maximum.

The energy flux of atmospheric turbulence is best described by the *energy cascade theory* that was introduced by L. F. Richardson in 1926: At large scales, the source of energy is either wind shear or convection. The wind speed increases until a critical Reynoldsnnumber is exceeded, resulting in local unstable air masses, also called eddies. These eddies are slightly smaller and independent of the parent flow. Their typical dimension is called the *outer scale of turbulence* L_0 , and they were found to be as large as 20 m or more⁴ [15, 16]. Under the influence of inertial forces, these large eddies brake up into smaller ones, who brake up on their part and so on, until they reach a minimum scale size, the *inner scale of turbulence* l_0 . Measurements have shown that this scale size is on the order of 5 mm to 12 mm [8]. Eddies of scale sizes between the outer and the inner scale form the *inertial subrange*. Scale sizes that are smaller than l_0 belong to the *viscous dissipation range*. In this range, the turbulent eddies disappear and the energy is dissipated as heat [6]. Richardson’s energy cascade model is visualized in Fig. 4.2.

³The kinematic viscosity is defined by $\nu = \mu/\rho$, where μ is the absolute viscosity and ρ is the density of the medium. The density of the atmosphere decreases with height, so ν increases, and the Reynoldsnnumber decreases, too, leading to more or less stable conditions in higher regions, like in the stratosphere and layers above.

⁴The outer scale of turbulence is generally much larger than the diameter of an observing telescope, so the actual value is not of great importance.

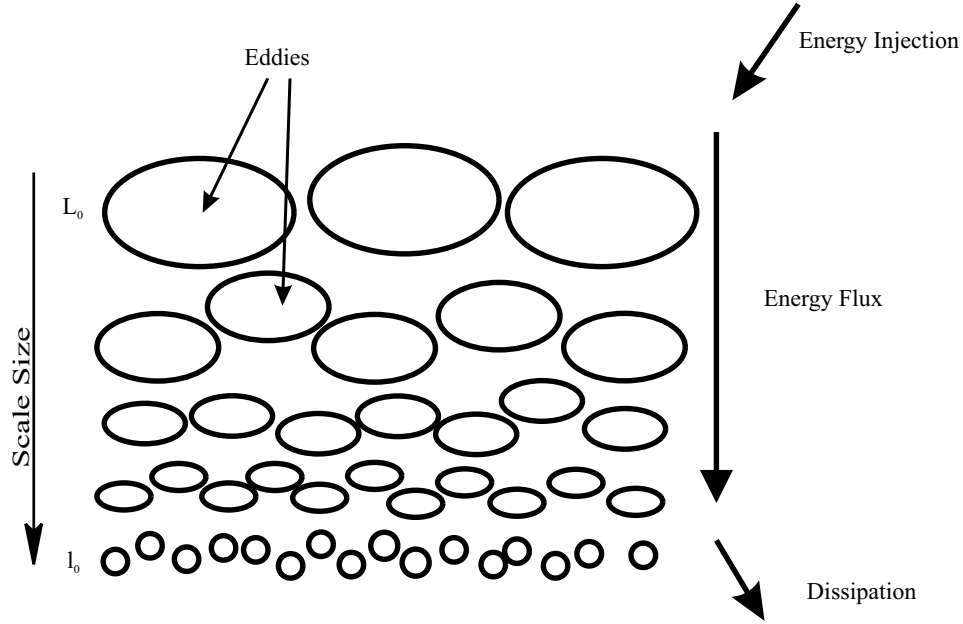


Figure 4.2: Richardson's energy cascade model; L_0 denotes the outer scale, and l_0 the inner scale of turbulence.

4.3 Structure Functions

Actual random (=stochastic) processes can often be approximated by stationary random functions. Unfortunately, this approximation is not justifiable with atmospheric parameters, like temperature fluctuations or changes in the wind velocity, because their mean values are constant only over relatively short periods of time.

To circumvent this problem, it is useful to analyze the behavior of the difference $x(t + \tau) - x(t)$ rather than that of the stochastic process $x(t)$ itself (t represents an arbitrary point in time, τ is an arbitrary time delay). The advantage of this method is that the difference $x(t + \tau) - x(t)$ often behaves like a stationary function, even though $x(t)$ may not be stationary. This method is also called the *method of stationary increments*⁵ [6].

The wide-sense description of a stochastic process is defined by its covariance function and its mean [17]. Since it is not always possible to find the corresponding covariance function, it is useful to introduce *structure functions*,

$$D_x(t, \tau) = \left\langle [x(t + \tau) - x(t)]^2 \right\rangle, \quad (4.2)$$

where $\langle \cdot \rangle$ denotes the ensemble average. Splitting the random process $x(t)$ into the mean $m(t) = \langle x(t) \rangle$ and a mean-free fluctuating part $x_1(t)$, the structure function can be written as

$$\begin{aligned} D_x(t, \tau) &= [m(t + \tau) - m(t)]^2 + \left\langle [x_1(t + \tau) - x_1(t)]^2 \right\rangle \\ &\approx \left\langle [x_1(t + \tau) - x_1(t)]^2 \right\rangle. \end{aligned} \quad (4.3)$$

⁵A random process is random with stationary increments if the ensemble averages of $[x(t + \tau) - x(t)]$ and $[x(t + \tau) - x(t)]^2$ are independent of the absolute instant t .

In the last step, it is assumed that the mean does not change significantly during the time of observation τ .

For random processes with stationary increments, the structure function $D_x(t, \tau)$ becomes independent of the absolute instant t , $D_x(t, \tau) = D_x(\tau)$.

If $x(t)$ is a stationary random process as well, then its covariance function $B_x(\tau)$ and its structure function are directly related:

$$\begin{aligned} D_x(\tau) &= \langle [x(t + \tau) - x(t)]^2 \rangle \\ &= \langle x^2(t + \tau) \rangle + \langle x^2(t) \rangle - 2 \langle x(t + \tau) - x(t) \rangle \\ &= 2[B_x(0) - B_x(\tau)] \end{aligned} \quad (4.4)$$

Note that it is impossible to derive the covariance function from the structure function!

A spatial equivalent for a random process with stationary increments is a field⁶ that is *locally homogeneous*⁷. Such a random field can be decomposed into a part with slowly varying mean and a mean-free fluctuating part,

$$x(\vec{r}) = m(\vec{r}) + x_1(\vec{r}). \quad (4.5)$$

These locally homogeneous fields are usually characterized by structure functions. Switching from the time domain to the spatial domain, (4.2) becomes

$$D_x(\vec{r}_0, \vec{r}) = \langle [x(\vec{r}_0 + \vec{r}) - x(\vec{r}_0)]^2 \rangle, \quad (4.6)$$

where \vec{r}_0 defines an arbitrary point in space, and \vec{r} is the difference vector that points from \vec{r}_0 to another arbitrary point. The spatial equivalent to (4.3) is

$$D_x(\vec{r}_0, \vec{r}) \approx \langle [x_1(\vec{r}_0 + \vec{r}) - x_1(\vec{r}_0)]^2 \rangle. \quad (4.7)$$

Spectral Representation

Many deterministic functions can be represented by their Fourier Spectra, $F(j\omega)$ ($\omega = 2\pi f$ is the angular frequency) [18]. A necessary condition for the existence of a Fourier spectrum is that the function is absolutely integrable,

$$\int_{-\infty}^{\infty} |f(t)| dt < \infty. \quad (4.8)$$

Using the Fourier transformation, it is possible to obtain a spectral representation of the time-dependent function,

$$F(j\omega) = \frac{1}{2\pi} \int_{-\infty}^{\infty} f(t) \exp[-j\omega t] dt. \quad (4.9)$$

The inverse Fourier transformation associates a frequency spectrum with a signal in the time domain,

$$f(t) = \int_{-\infty}^{\infty} F(j\omega) \exp[j\omega t] d\omega. \quad (4.10)$$

⁶A random function of a vector spatial variable $\vec{r} = x\vec{e}_x + y\vec{e}_y + z\vec{e}_z$ and, possibly, time t is called random field.

⁷A field is called locally homogeneous if its moments are invariant under spatial translation.

From (4.9), one can see that the corresponding spectrum will normally be complex valued, except when the signal in the time domain is an even function, leading to a real valued spectrum.

For complex stationary random functions $x(t)$, condition (4.8) will not be met. To obtain a spectral representation, the *Fourier–Stieltjes integral* has to be involved,

$$x(t) = \int_{-\infty}^{\infty} \exp[j\omega t] d\nu(\omega), \quad (4.11)$$

where $d\nu(\omega)$ is a random complex amplitude, and $\langle x(t) \rangle = 0$. Of course, $x(t)$ and $d\nu(\omega)$ differ for each realization of the random process. Therefore, the power spectral density can be used to describe the random process in the frequency domain [17]. It is obtained by taking the Fourier transform of the autocorrelation function, which is equal to the covariance function, since the random process is mean free.

Using (4.11), the covariance function can be expressed as ($t_{1,2}$ are independent points in time)

$$B_x(t_1, t_2) = \langle x(t_1)x^*(t_2) \rangle \quad (4.12)$$

$$= \iint_{-\infty}^{\infty} \exp[j(\omega_1 t_1 - \omega_2 t_2)] \langle d\nu(\omega_1) d\nu^*(\omega_2) \rangle, \quad (4.13)$$

where $\omega_{1,2}$ are auxiliary variables of frequency. With regard to random processes with stationary increments, the correlation function must not be a function of an absolute instant, so the random amplitude has to satisfy

$$\langle d\nu(\omega_1) d\nu^*(\omega_2) \rangle = \delta(\omega_2 - \omega_1) S_x(\omega_1) d\omega_2 d\omega_1, \quad (4.14)$$

where $S_x(\omega_1) \geq 0$ is the *power spectral density* of the stochastic process $x(t)$. Replacing ω_1 by ω and τ by $t_1 - t_2$, (4.13) becomes

$$B_x(\tau) = \int_{-\infty}^{\infty} S_x(\omega) \exp[j\omega\tau] d\omega. \quad (4.15)$$

The power spectral density is the inverse Fourier transform of the covariance function,

$$S_x(\omega) = \frac{1}{2\pi} \int_{-\infty}^{\infty} B_x(\tau) \exp[-j\omega\tau] d\tau. \quad (4.16)$$

This set of equations, (4.15) and (4.16), is known as the *Wiener–Khinchine theorem*.

A locally homogeneous stochastic field $x(\vec{r})$ is usually described by its structure function, (4.7), rather than by its covariance function. It is also possible to derive a relation between the structure function and its power spectrum $\Phi_n(\vec{\kappa})$ [6, 19],

$$D_x(\vec{r}) = 2 \int_{-\infty}^{\infty} \Phi_x^2(\vec{\kappa}) [1 - \cos(\vec{\kappa} \cdot \vec{r})] d\vec{\kappa}. \quad (4.17)$$

The power spectrum $\Phi_n(\vec{\kappa})$ is the spatial equivalent of $S_x(\omega)$, as $\vec{\kappa}$ (in radians/meter) is to ω . In other words, κ can be interpreted as a spatial frequency.

If the locally homogeneous stochastic field is isotropic, (4.17) simplifies to

$$D_x(r) = 8\pi \int_0^\infty \kappa^2 \Phi_x(\kappa) \left(1 - \frac{\sin(\kappa r)}{\kappa r}\right) d\kappa, \quad (4.18)$$

with $r = |\vec{r}|$ and $\kappa = |\vec{\kappa}|$.

The equivalent to (4.16) is [6]

$$\Phi_x(\kappa) = \frac{1}{4\pi^2 \kappa^2} \int_0^\infty \frac{\sin(\kappa r)}{\kappa r} \frac{d}{dr} \left[r^2 \frac{d}{dr} D_x(r) \right] dr. \quad (4.19)$$

The spectra of the structure functions are included in approximations for the moments of the field. Using the moments, one can calculate the impacts on a laser beam passing through random media (see Chap. 5).

4.4 Spectra of Turbulence

Turbulence is a nonlinear process that can be described by the Navier–Stokes equations. A. N. Kolmogorov had difficulties solving these equations, so he developed a statistical theory of turbulence that relied on dimensional analysis [20]. In other words, his results were obtained empirically, they were not derived from basic assumptions. Since his work is fundamental for other considerations, the description of turbulence that is commonly used relies on empirical data.

For locally homogeneous, isotropic turbulence, Kolmogorov showed that the wind velocity parallel to a vector \vec{r} connecting two observation points obeys a “2/3” power law,

$$D_v(r) = C_v^2 r^{2/3}, \quad l_0 \ll r \ll L_0, r = |\vec{r}|. \quad (4.20)$$

The *structure constant* C_v^2 represents the total amount of the wind’s energy in turbulence. It is related to the average energy dissipation rate ϵ by $C_v^2 = 2\epsilon^{2/3}$. The inner scale $l_0 \approx \eta = (\nu^3/\epsilon)^{1/4}$ depends on the kinematic viscosity ν and the average rate of dissipation ϵ . The parameter η is *Kolmogorov’s microscale*. The outer scale of turbulence, L_0 , is proportional to $\sqrt{\epsilon}$. For separation distances r smaller than l_0 ,

$$D_v(r) = C_v^2 l_0^{4/3} r^2, \quad r \ll l_0. \quad (4.21)$$

No general description of the structure function can be predicted for separation distances larger than the outer scale L_0 , since the velocity fluctuations are nonisotropic and local homogeneity is not warranted.

The corresponding power spectrum can be derived from (4.19) [6],

$$\Phi_v(\kappa) = 0.033 C_v^2 \kappa^{-11/3}, \quad 1/L_0 \ll \kappa \ll 1/l_0. \quad (4.22)$$

This spectrum is plotted in Fig. 4.3. Most of the energy lies at large scale sizes (where κ is small), descending to lower scale sizes.

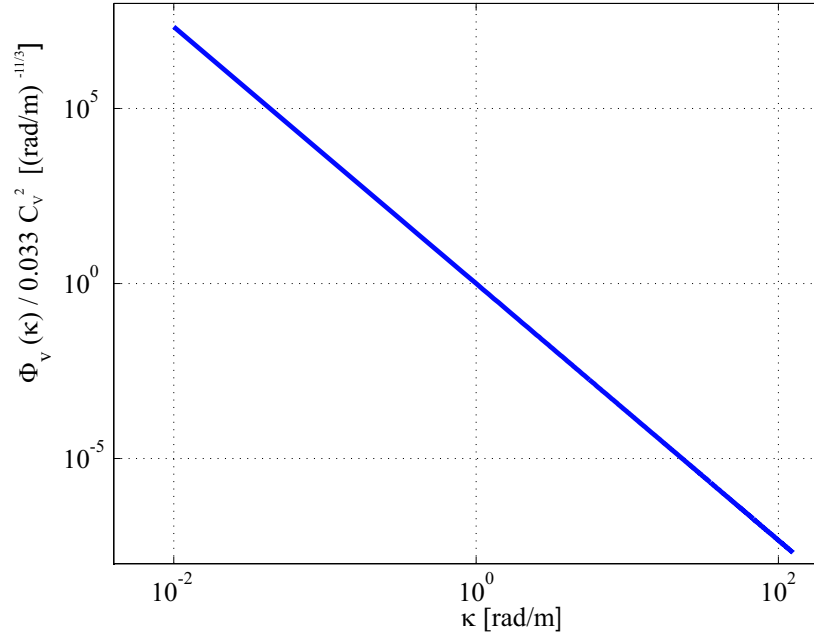


Figure 4.3: Double logarithmic plot of the normalized power spectrum of the wind velocity in the region $1/L_0 < \kappa < 1/l_0$ ($L_0 = 100$ m, $l_0 = 8$ mm).

The considerations above can also be adapted to temperature fluctuations [6]. The necessary conditions are that the fluctuations of the temperature are locally homogeneous and isotropic. Meeting these conditions, (4.22) takes on the form

$$\Phi_T(\kappa) = 0.033 C_T^2 \kappa^{-11/3}, \quad 1/L_0 \ll \kappa \ll 1/l_0. \quad (4.23)$$

The only differences between (4.23) and (4.22) are the structure constant, and the definition of the inner scale size. For temperature fluctuations, the inner scale is defined by $l_0 = 5.8(D^3/\epsilon)^{1/4}$, where D is the diffusivity of heat in air (in m^2/s). The magnitude of the inner scale of temperature fluctuations is of the same order as that of velocity fluctuations.

Temperature fluctuations and fluctuations of the index of refraction are closely related. For locally homogeneous and isotropic turbulence, the following structure function can be defined:

$$D_n(r) = \begin{cases} C_n^2 r^{2/3}, & l_0 \ll r \ll L_0, \\ C_n^2 l_0^{-4/3} r^2, & r \ll l_0. \end{cases} \quad (4.24)$$

The inner scale of turbulence is defined by $l_0 = 7.4\eta = 7.4(\nu^3/\epsilon)^{1/4}$, and C_n^2 is the index of refraction's *structure parameter*. The structure parameter represents the strength of the fluctuations of the refractive index. The close relation of the refractive index to the temperature fluctuations leads to a simple rule to transfer C_T^2 into C_n^2 , using (3.4):

$$C_n^2 = 77.6 \cdot 10^{-8} \left(1 + \frac{7.52 \cdot 10^{-15} \text{ m}^2}{\lambda^2} \right) \frac{p}{T^2} C_T^2 \frac{\text{ms}^2 \text{K}^2}{\text{kg}}. \quad (4.25)$$

Here, p is the pressure in Pascal, T is the temperature in Kelvin, λ is the wavelength in m, and C_T^2 is the structure parameter of the temperature fluctuations in $\text{m}^{-2/3}$. Based on (4.23),

the power spectrum of the refractive index's fluctuations in the inertial subrange becomes

$$\Phi_n(\kappa) = 0.033C_n^2\kappa^{-11/3}, \quad 1/L_0 \ll \kappa \ll 1/l_0. \quad (4.26)$$

This equation is the well-known *Kolmogorov spectrum*, which is, because of its simplicity, widely used in theoretical considerations⁸. All spectra presented in this thesis have in common the Kolmogorov spectrum of turbulence over a major part of the inertial subrange. The Kolmogorov spectrum is plotted as the straight dashed line in Fig. 4.4.

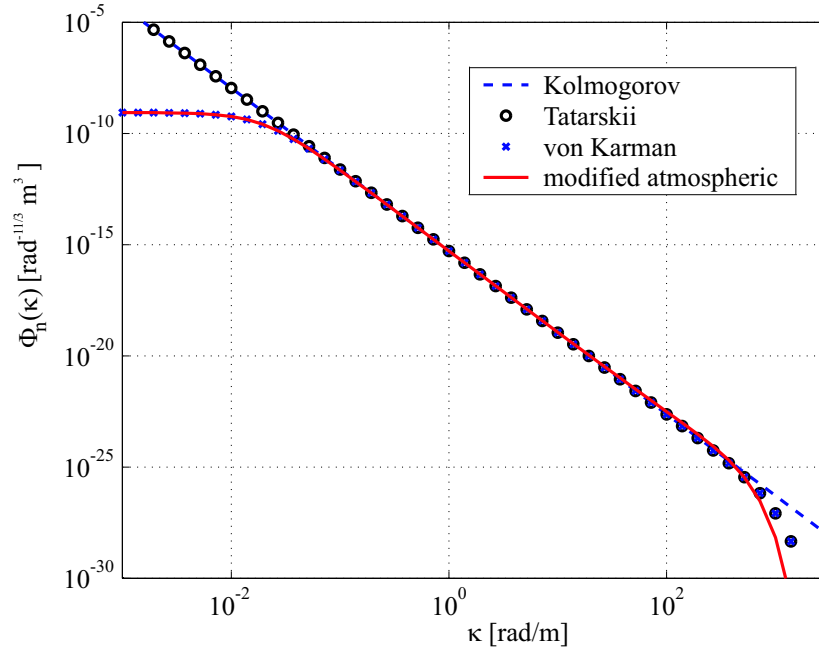


Figure 4.4: Models for the spectrum of the refractive index's fluctuations ($L_0 = 50$ m, $l_0 = 8$ mm). The area $1/L_0 \dots 1/l_0$ is the inertial subrange.

Tatarskii Spectrum: Tatarskii [4] extended Kolmogorov's spectrum so that it was also valid in the dissipation range, i.e., where $\kappa > 1/l_0$. To this end, (4.26) is multiplied by a Gaussian function to truncate the spectrum at high wavenumbers,

$$\Phi_n(\kappa) = 0.033C_n^2\kappa^{-11/3} \exp[-\kappa^2/\kappa_m^2], \quad \kappa \gg 1/L_0. \quad (4.27)$$

The parameter κ_m is $5.92/l_0$. At low wavenumbers, this model equals Kolmogorov's spectrum (see Fig. 4.4, curve marked by 'o'). A disadvantage of the Kolmogorov and the Tatarskii spectrum is their singularity at $\kappa = 0$. This singularity is a discrepancy between the mathematical model and real turbulence: while atmospheric turbulence is almost always locally homogeneous and isotropic, the Kolmogorov and the Tatarskii spectra contain these properties only in the inertial subrange or dissipation range for which $\kappa \gg 1/L_0$.

⁸Zilberman *et al.* have shown by measurements that the Kolmogorov spectrum has to be modified above the atmospheric boundary layer, i.e., approximately 1km above the earth's surface [21]. This has not been included in this thesis.

von Kármán Spectrum: The Kolmogorov and the Tatarskii spectrum are not capable of describing atmospheric turbulence at low wavenumbers, i.e., where $\kappa < 1/L_0$. This leads to the shortcoming that, e.g., the covariance function does not exist. A model that overcomes this problem is the von Kármán spectrum:

$$\Phi_n(\kappa) = 0.033C_n^2 \frac{\exp[-\kappa^2/\kappa_m^2]}{(\kappa^2 + \kappa_0^2)^{11/6}}, \quad 0 \leq \kappa \leq \infty \quad (4.28)$$

with $\kappa_m = 5.92/l_0$ and $\kappa_0 = 1/L_0$. In Fig. 4.4, where the profile of the von Kármán spectrum is marked by \times , it can be seen that, at high wavenumbers, this type of spectrum follows the Tatarskii spectrum, while at low wavenumbers, it flattens and takes on a constant value.

Modified Atmospheric Spectrum: Experiments have shown that there exists a slight bump in the spectrum at high wavenumber (around $1/l_0$) [6]. This bump is unattended by all presented models. The only spectrum that takes it into account is the modified atmospheric spectrum [6],

$$\Phi_n(\kappa) = 0.033C_n^2 \left[1 + 1.802(\kappa/\kappa_l) - 0.254(\kappa/\kappa_l)^{7/6} \frac{\exp[-\kappa^2/\kappa_l^2]}{(\kappa^2 + \kappa_0^2)^{11/6}} \right], \quad 0 \leq \kappa \leq \infty \quad (4.29)$$

where $\kappa_l = 3.3/l_0$ and $\kappa_0 = 1/L_0$. The modified atmospheric spectrum is the solid curve in Fig. 4.4.

4.4.1 The Structure Parameter C_n^2

The structure parameter C_n^2 represents the total amount of energy contained in the stochastic field of the refractive index's fluctuations⁹. Because of the spatial dependency of the structure parameter, it will be written in a parameterized version, $C_n^2(z)$, where z represents the relative distance to the starting point of observation.

The values of $C_n^2(z)$ can be determined indirectly by the structure parameter for temperature fluctuations $C_T^2(z)$. This structure parameter can then be converted using (4.25). Note that the pressure and the temperature in (4.25) are also location dependent.

One possibility to measure $C_T^2(z)$ is to keep two fine wire thermometers at a fixed distance r and to record the mean-square temperature difference. Using the definition of the structure function for temperature fluctuations,

$$D_T(r, z) = C_T^2(z)r^{2/3}, \quad (4.30)$$

the structure parameter $C_T^2(z)$ can be determined. (The value of $D_T(r, z)$ is measured, and the separation distance r of the two fine wire probes is determined, e.g. $r = 1$ m.)

Another way to obtain the $C_n^2(z)$ profile is by using the SCIDAR (SCIntillation Detection And Ranging) technique. The light from stars is used to calculate a correlation function. The height and strength of any turbulent layer can be determined from the peaks of this function (see [22] for further information, and [23] for sample measurements).

Path-averaged values of $C_n^2(z)$ and of the inner scale of turbulence $l_0(z)$ can be measured with an instrument called scintillometer, like those in Fig. 4.5. This device uses a *Shack-Hartman wavefront sensor* to measure local variations (or *scintillations*) over the cross section of a laser beam (see, e.g., [24] for an introduction to Shack-Hartman wavefront sensors).

⁹Another name is structure constant, but this notation is physically not correct, since C_n^2 is constant only in a relatively small area.



Figure 4.5: Optical Scintillometers, ©Scintec AG, Germany, <http://www.scintec.com/>

The structure parameter $C_n^2(h)$ is also a function of time. The temperature near the earth's surface varies with time because of the change in solar radiation:

Day: The earth's surface is generally warmer than the air above, leading to strong wind and strong turbulences. Averaged values for $C_n^2(0)$ (near ground) reach from $10^{-14} \text{ m}^{-2/3}$ to $10^{-11} \text{ m}^{-2/3}$ ("strong turbulence")

Night: More stable conditions can be expected since the air is warmer than the ground. Values for $C_n^2(0)$ are from $10^{-15} \text{ m}^{-2/3}$ to $10^{-13} \text{ m}^{-2/3}$

Morning / Evening: The temperature of air and ground are almost equal, the most stable conditions can be expected. Values for $C_n^2(0)$ of $10^{-16} \text{ m}^{-2/3}$ or less are possible ("weak turbulence").

The range for values of the structure parameter C_n^2 is highly location dependent, thus may differ from the values above, but the cycle over daytime will be the same.

The troposphere (see Sect. 4.1) has the biggest impact on the structure parameter, both for horizontal and slant or vertical $C_n^2(z)$ profiles.

Models for $C_n^2(h)$

There exist several models for the calculation of the vertical profile of the structure parameter:

Hufnagel–Valley (H–V) Model: This model is based on measurements that were made at various locations [6]. It is a good approximation for the behaviour of $C_n^2(h)$ (the parameter h indicates the height). An advantage of this model is that only two measured values are needed: the rms-windspeed¹⁰ v in m/s, and the value of C_n^2 near ground (at $h = 0$).

$$C_n^2(h) = 0.00594(v/27)^2(10^{-5}h)^{10} \exp(-h/1000) + 2.7 \times 10^{-16} \exp(-h/1500) + C_n^2(0) \exp(-h/100) \quad (4.31)$$

¹⁰The root mean square windspeed is calculated as follows: $v = \sqrt{\frac{1}{15 \cdot 10^3} \int_{5 \cdot 10^3}^{20 \cdot 10^3} V^2(h) dh}$ with $V(h) = v_g + 30 \exp[-((h - 9400)/4800)^2]$. v_g is the wind speed near ground. If the direction of the path along which the C_n^2 -profile is specified changes, this has to be taken into account by adding a term $\omega_s h$ to $V(h)$. The variable ω_s is the slew rate associated with that motion.

Choosing $v = 21$ m/s and $C_n^2(0) = 1.7 \cdot 10^{-14} \text{ m}^{-2/3}$ yields the commonly used Hufnagel–Valley_{5/7} (H–V_{5/7}) profile. The index 5/7 comes from values that are reached using this model: For a wavelength of $\lambda = 0.5 \mu\text{m}$, the atmospheric coherence diameter (= two times the atmospheric coherence length presented in Sect. 3.2) becomes 5 cm, and the isoplanatic angle becomes $7 \mu\text{rad}$ (the isoplanatic angle is the aperture angle of a beam in which the profile of $C_n^2(h)$ is constant). Figure 4.6 shows the H–V model for different values of $C_n^2(0)$ and v . The bump at a height of 10 000 meters comes from a region with high wind velocities (up to 400 km/h). These winds are called jet streams [25].

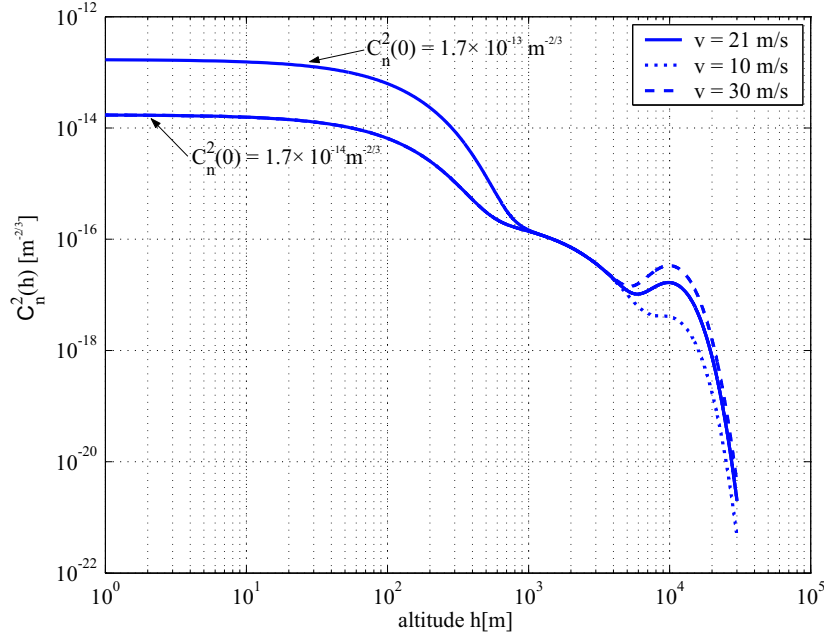


Figure 4.6: Profile for $C_n^2(h)$ after Hufnagel and Valley (H–V) ($v = 21$ m/s and $C_n^2(0) = 1.7 \cdot 10^{-14}$ correspond to the H–V_{5/7} model).

CLEAR 1: Depending on the height above ground h , this model provides different equations to determine the value of $C_n^2(h)$ [26]. No measured data is needed:

$$\begin{aligned}
 \log_{10}(C_n^2) &= A_1 - B_1 h + C_1 h^2 & 1230 \leq h \leq 2130 \\
 \log_{10}(C_n^2) &= A_2 - B_2 h + C_2 h^2 & 2130 \leq h \leq 10340 \\
 \log_{10}(C_n^2) &= A_3 - B_3 h + C_3 h^2 \\
 &\quad + D e^{-0.5(\frac{h-E}{F})^2} & 10340 \leq h \leq 30000
 \end{aligned} \tag{4.32}$$

The parameters $A_i \dots F$ can be found at [26]. Figure 4.7 shows a plot of (4.32), along with a measured profile of $C_n^2(h)$. Since no meteorological data is used, the CLEAR1 model is the worst approximation of the measured $C_n^2(h)$ profile.

SLC Day and Night Model: SLC stands for *submarine laser communication studies*. The *SLC Day Model* is based on daytime averages. It is defined by [6]

$$C_n^2(h) = \begin{cases} 1.7 \cdot 10^{-14} \text{ m}^{-2/3}, & \dots \quad 0 \text{ m} < h < 18.5 \text{ m}, \\ 3.13 \cdot 10^{-13} / h^{1.05} \text{ m}^{-2/3}, & \dots \quad 18.5 \text{ m} < h < 240 \text{ m}, \\ 1.3 \cdot 10^{-15} \text{ m}^{-2/3}, & \dots \quad 240 \text{ m} < h < 880 \text{ m}, \\ 8.87 \cdot 10^{-7} / h^3 \text{ m}^{-2/3}, & \dots \quad 880 \text{ m} < h < 7200 \text{ m}, \\ 2.0 \cdot 10^{-16} \text{ m}^{-2/3}, & \dots \quad 7200 \text{ m} < h < 20000 \text{ m}. \end{cases} \quad (4.33)$$

The *SLC Night Model* differs from the SLC Day model only below altitudes of 1500m. It is given by

$$C_n^2(h) = \begin{cases} 8.4 \cdot 10^{-15} \text{ m}^{-2/3}, & \dots \quad 0 \text{ m} < h < 18.5 \text{ m}, \\ 2.87 \cdot 10^{-12} \text{ m}^{-2/3} / h^2, & \dots \quad 18.5 \text{ m} < h < 240 \text{ m}, \\ 2.5 \cdot 10^{-16} \text{ m}^{-2/3}, & \dots \quad 240 \text{ m} < h < 880 \text{ m}, \\ 8.87 \cdot 10^{-7} / h^3 \text{ m}^{-2/3}, & \dots \quad 880 \text{ m} < h < 7200 \text{ m}, \\ 2.0 \cdot 10^{-16} \text{ m}^{-2/3}, & \dots \quad 7200 \text{ m} < h < 20000 \text{ m}. \end{cases} \quad (4.34)$$

This model uses median values of $C_n^2(h)$ above the Air Force Maui Optical Station (AMOS) in Hawaii, thus may not be representative for other geographical locations.

Dewan: The Dewan model uses meteorological data to predict the $C_n^2(h)$ profile [26]. The air pressure, temperature, height, and the outer scale of turbulence are used to approximate values for $C_n^2(h)$. Figure 4.7, shows that the Dewan model follows the measured profile most precisely.

HMNSP99: The abbreviation HMSNP99 stands for HollowMaN SPring 99, that is the location where the measurements that led to the model were made. Like Dewan, this model involves meteorological data to predict the $C_n^2(h)$ profile [26]. The difference to the Dewan model lies in the approximation of the outer scale of turbulence. HMNSP99 has the smallest statistical error among all models, but as can be seen in Fig. 4.7, green line, it is not as good as Dewan in approximating the real distribution of C_n^2 .

4.5 Classification of the Turbulent Environment

The structure parameter $C_n^2(h)$ is used to determine the magnitude of the turbulence. A commonly used method to classify the strength of turbulence is to use the *scintillation index*,

$$\sigma_1 = 1.23 \tilde{C}_n^2 k^{7/6} L^{11/6}, \quad (4.35)$$

where k is the wavenumber, L is the propagation distance, and \tilde{C}_n^2 is the path-averaged value of $C_n^2(h)$. Turbulences are weak if $\sigma_1 \ll 1$, and strong if $\sigma_1 \geq 1$. I calculated the average of $C_n^2(h)$ by employing an integral form of the arithmetic mean,

$$\tilde{C}_n^2 = \frac{\int_0^L C_n^2(h) dh}{\int_0^L dh}. \quad (4.36)$$

As an example, inserting the H-V_{5/7} profile for $C_n^2(h)$ and choosing vertical propagation for the path integral yields $\tilde{C}_n^2 = 2.19 \cdot 10^{-23} \text{ m}^{-2/3}$ for a distance of $L = 450 \text{ km}$. For $\lambda = 1.55 \mu\text{m}$, I yield $\sigma_1 = 3.23 \cdot 10^{-4}$, so this turbulent environment can be considered weak.

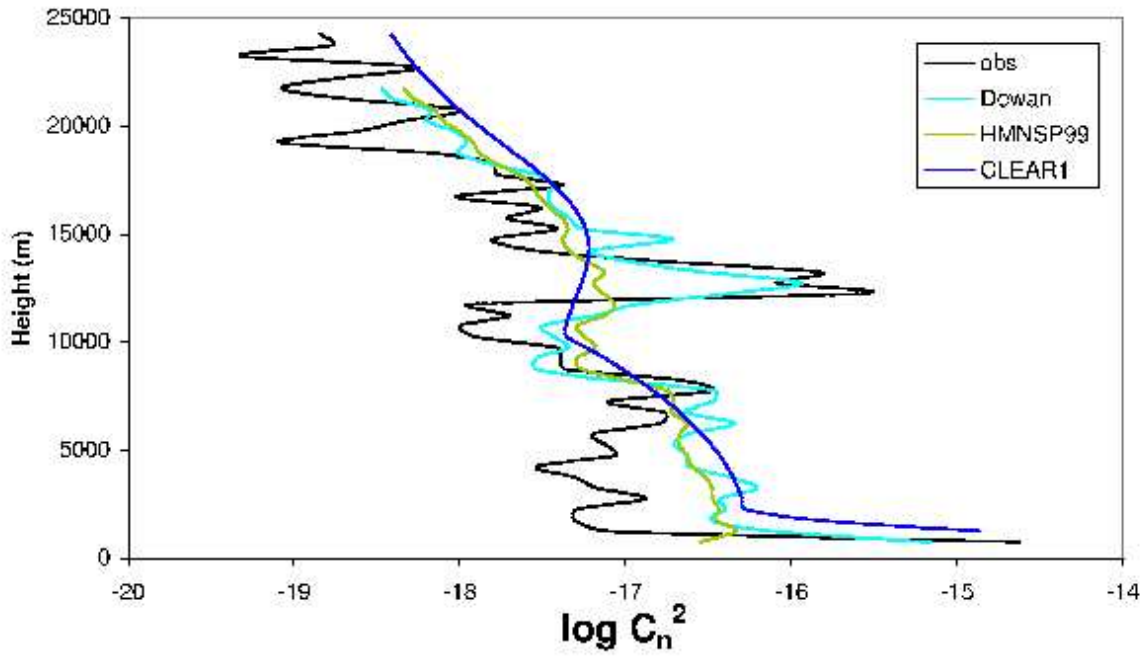


Figure 4.7: Comparison of $C_n^2(h)$ models that use meteorological data. The thin line shows the measured profile. The Dewan model follows the measured values most precisely, while the HMNSP99 model has the smallest statistical error (from [26]).

Chapter 5

Results

The fundamentals for the analysis of the behavior of an optical wave propagating through turbulent media were presented in the preceding chapters.

In this chapter, qualitative results are derived and applied to the following scenario: A Gaussian beam (cf. Sect. 2.3) emerges from an optical ground station vertically into space, where a receiver is located at a low earth orbit (LEO) satellite (altitude: 450km) (uplink). The beam is disturbed at the very beginning of the propagation path, when it passes through the lowest layer of the atmosphere. This layer is characterized weakly turbulent, cf. Sect. 4.5. On the other hand, when the LEO satellite is the transmitter, the beam traverses the troposphere at the end of the propagation path (downlink). The location of the disturbing element, the troposphere (cf. Sect. 4.1), is different for the uplink and the downlink, so impacts of different orders can be expected.

The troposphere contains eddies of scale sizes from l_0 to L_0 , which are the inner and the outer scale of turbulence, respectively (Sect. 4.2). Each eddy is an area of nearly constant refractive index n (Sect. 3.1). A demonstrative illustration of the turbulent atmosphere is given by the following figure: Atmospheric turbulence can be interpreted as a continuum of lenses with random focal lengths. These lenses are responsible for the displacement of the beam (*Beam Wander*), and for a broadening of the beam (*Short-Term Beamspread*) in addition to free space spreading (see Sect. 2.3).

5.1 Absorption

Air is a mixture of various gases and particles. When a laser beam passes through the atmosphere, the atmospheric constituents such as water vapor, carbon dioxide, and ozone absorb parts of its energy. The transmission of air is plotted in Fig. 5.1. The narrow regions where the atmospheric transmission reaches very low values in Figure 5.1 reveal that molecular absorption is rather a thin line than a band phenomenon [27].

The order of magnitude of atmospheric absorption depends on the weather conditions. For clear air, the attenuation will be some 1–2 dB at a wavelength of $1.55\text{ }\mu\text{m}$.

5.2 Scattering

Small particles in the atmosphere deflect the laser beam in various directions. This effect atmospheric impact is called Rayleigh scattering. For objects that are larger than the wavelength, Mie scattering occurs. While the dependency on the wavelength is given by λ^{-4} for

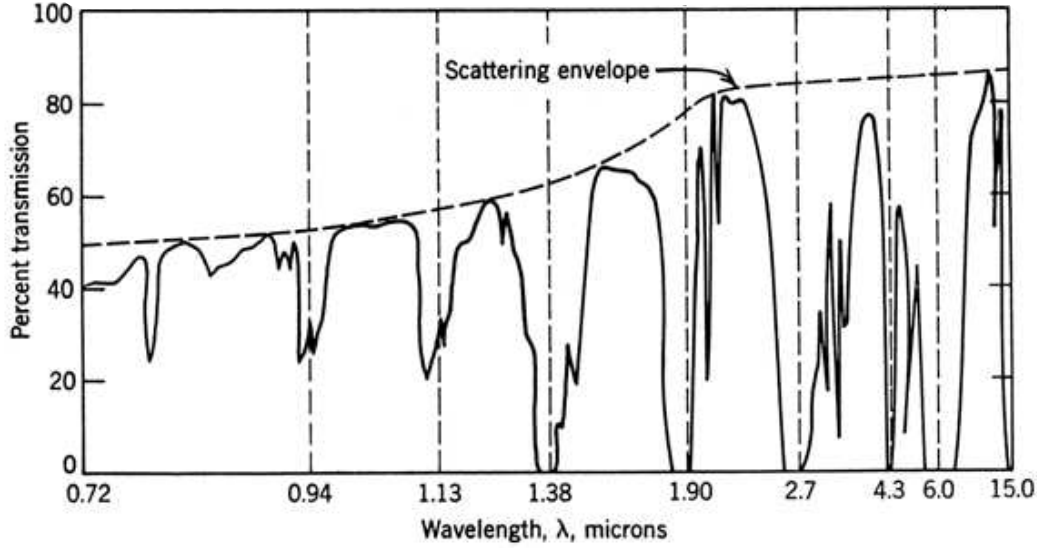


Figure 5.1: Transmission of the atmosphere as a function of the wavelength (from[27]).

Rayleigh scattering, Mie scattering does not depend on the wavelength that strong. The curve in Figure 5.1 represents measurements of both absorption and scattering [27].

5.3 Beam Wander

The Gaussian beam has a well-defined diameter at each point along its propagation direction. This diameter $2w(L)$ (2.40) depends on the initial diameter $2w_0$ of the beam waist, on the wavelength λ , and on the propagation distance L ,

$$2w(L) = 2(w_0 + \theta_0 L) = 2 \left(w_0 + \frac{\lambda}{\pi w_0} L \right). \quad (5.1)$$

Generally, aperture effects will also lead to an additional broadening of the beam, but these effects are not analyzed within this thesis.

For the uplink case, the beam is immediately affected by the turbulent troposphere. As described before, this layer of the atmosphere consist of eddies with different scale sizes that can be interpreted as lenses. When the beam impinges on an eddy that is of a larger size than the beam's diameter, the direction of the beam will be altered, like shown in Fig. 3.1.

For the downlink case, the beam will already be much larger than most of the eddies because of diffraction.

Therefore, negligible beam wander is expected for the downlink, while for the uplink, there should be a noticeable displacement.

The distribution of the intensity of the laser beam will not retain its Gaussian form when passing through turbulence [3, 4, 6]. I assumed that the laser beam remains Gaussian in the approximations presented within this thesis. This is justified since many approaches have been made in the same way, leading to results that were confirmed by experiments (horizontal propagation) [1, 3, 4, 6]. Therefore, the maximum of the intensity of the laser beam will be at the center of the laser beam's profile (orthogonal to the propagation direction). The

displacement of this center $\rho_c(h)$ at a certain height h can be found by calculating the center of gravity of the irradiance $I(\vec{\rho}, h)$ ($\vec{\rho}$ is the vector from the observed point to the geometrical middle of the area, that is, the spot where the maximum would be located if there were no turbulence),

$$\rho_c(h) = \frac{\int_0^\infty \vec{\rho} I(\vec{\rho}, h) d\vec{\rho}}{\int_0^\infty \langle I(\vec{\rho}, h) \rangle d\vec{\rho}}. \quad (5.2)$$

Figure 5.2 shows the spot of the laser beam without turbulence (at the center of the figure) and the displaced laser beam.

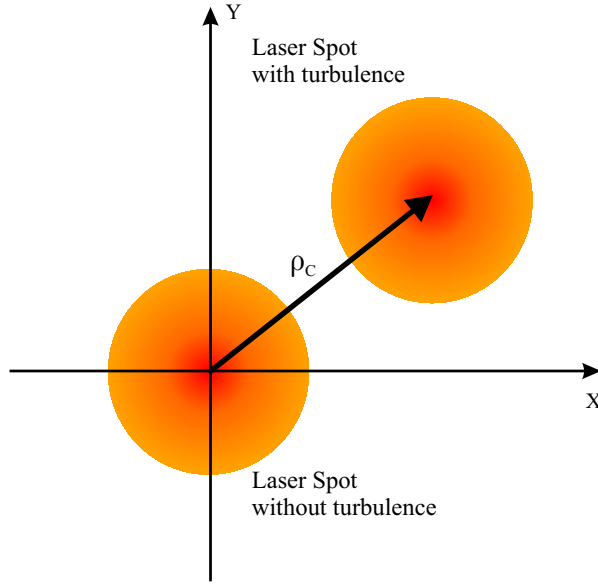


Figure 5.2: Displacement of the center of the beam due to turbulence (= beam wander)

With the moments of the field (Chapt. 3), (5.2) can be transformed into [3, 9]

$$\langle \rho_c^2(h) \rangle = \frac{\int_0^\infty \int_0^\infty (\vec{\rho}_1 \cdot \vec{\rho}_2) \Gamma_{2,2}(\vec{\rho}_1, \vec{\rho}_1, \vec{\rho}_2, \vec{\rho}_2; h) d\vec{\rho}_1 d\vec{\rho}_2}{\left[\int_0^\infty \Gamma_{1,1}(\vec{\rho}_1, \vec{\rho}_1; h) d\vec{\rho}_1 \right]^2}. \quad (5.3)$$

Solutions for $\Gamma_{1,1}$, the second order moment of the field, are known [3, 9], but there exist only limited approximations for the fourth order moment $\Gamma_{2,2}$. Since it is possible to calculate the maximum radius of the beam wander more easily (i.e., without using the moments of the field), I will present the results of this method.

Sasiela analytically derived an equation for the beam wander $\rho_C(L)$ [1]. He used the Rytov method to get an expression for the log-amplitude variance¹, which he solved by Mellin

¹The amplitude of the irradiance after passing through turbulence is assumed to be distributed log-normally, and the phase's distribution to be uniform.

transformation methods. Andrews and Phillips adapted these results and simplified them, yielding [6]

$$\langle \rho_C^2 \rangle = \begin{cases} 2.87L^2w_0^{-1/3} \int_0^L C_n^2(h)dh & \text{(Uplink)} \\ 8.61w_0^{-1/3} \int_0^L C_n^2(h)h^2dh & \text{(Downlink)}. \end{cases} \quad (5.4)$$

The squareroots of ρ_C are plotted in Fig. 5.3 as a function of w_0 , which is the initial beam radius. The link distance is $L = 450$ km, and the Hufnagel–Valley_{5/7} model (H–V_{5/7}) is used for the profile of $C_n^2(h)$.

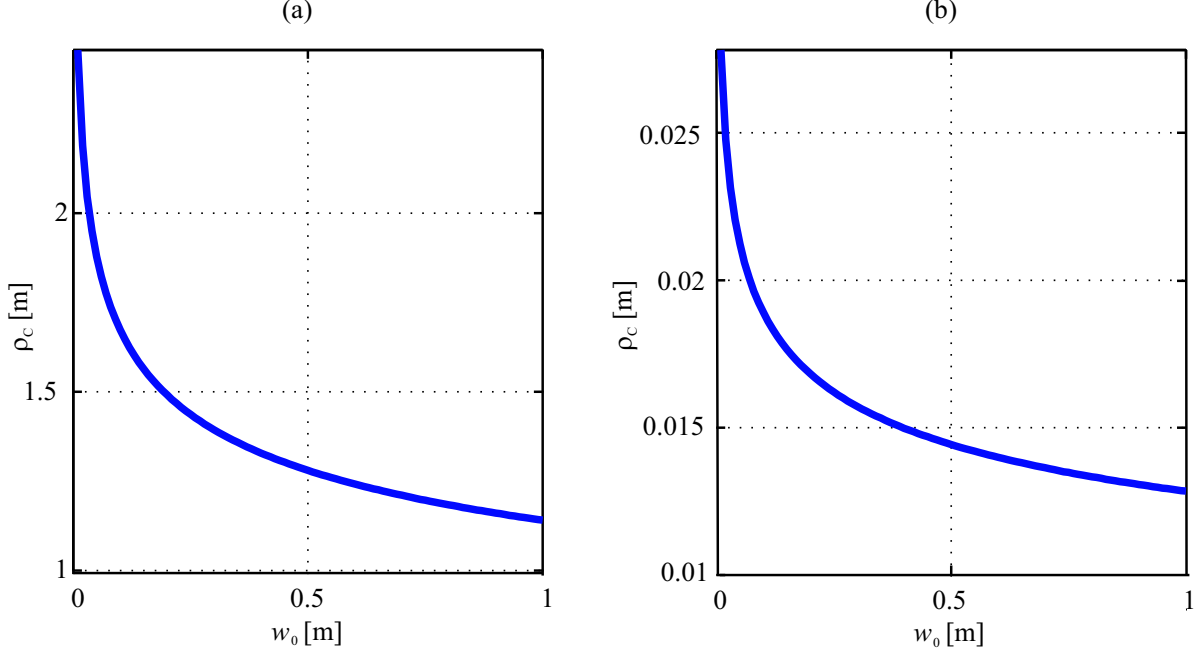


Figure 5.3: Beam Wander ρ_C using the Rytov Approximation; (a) Uplink, (b) Downlink

Figure 5.3 confirms the assumption that was made at the beginning of this section: while the beam wander must not be neglected for the uplink case, it can be neglected in the downlink case.

Klyatskin and Kon approximated a solution for (5.2) involving the Markov approximation [28]. They used degenerate hypergeometric functions (Kummer functions) to express the beam displacement ρ_C , but their calculations result in very high values for the beam wander. Depending on the initial beam waist, the beam wander would be on the order of 20 m to 40 m. Measurements lead to the conclusion that these results are implausible [3]. Since no range of validity for their formula is mentioned in [28], I analyzed various scenarios with different pathlengths and different strengths of $C_n^2(h)$, but never achieved physically reasonable results.

In the previous solutions, it is assumed that the Gaussian beam retains its initial shape. Fante suggests the possibility that the beam changes its shape, depending on the length of the propagation path (L) and the strength of turbulence [9]:

1. If $L \leq k \cdot A^2$, where k is the wavenumber and A is $\min[2w, \rho_0]$ ($2w$ is the beam diameter at the transmitter, and ρ_0 is the atmospheric coherence length (see Sect. 3.2)), the laser beam may behave as follows:

- (a) When $\rho_0 \ll 2w < L_0$, beam wander is determined by

$$\rho_C(L) = \sqrt{\frac{2.97L^2}{k^2\rho_0^{5/3}(2w)^{1/3}}}. \quad (5.5)$$

This expression is similar to (5.4), yielding almost the same results.

- (b) For the case when $\rho_0 \sim 2w$, there do not exist any analytic expressions for the beam wander, but it can be estimated from diagrams [9]. Another possibility to obtain values for this case is to subtract the short-term beamspread from the long-term beamspread. Both will be addressed in the next sections.
- (c) When $\rho_0 \gg 2w$, beam wander will be negligible.
2. If $L \gg k \cdot A^2$, the beam is expected to break up into multiple patches. It is not possible to define a measure for the beam wander.

The atmospheric coherence length can be calculated by [9]

$$\rho_0 = \left[1.46k^2 \int_0^L \left(1 - \frac{\eta}{L}\right)^{5/3} C_n^2(\eta) d\eta \right]^{-3/5}. \quad (5.6)$$

For the H-V_{5/7} profile, a propagation length of $L = 450$ km, and at the wavelength $\lambda = 1.55 \mu\text{m}$, the coherence length amounts to $\rho_0 \approx 9$ cm. Inserting these values into the above conditions shows that the second case will be met for most beams: $k \cdot \rho_0^2 \approx 33$ km $\ll 450$ km. The beam can be expected to “break up”, and as it is impossible to determine how many patches there will be, it is impossible to determine the beam wander. This behavior is similar to the picture shown in Fig. 5.4(b).

5.4 Short-Term Beamspread

Beam wander occurs when a laser beam is refracted by an eddy of a dimension that is larger than the beam’s diameter. Since there exist eddies of different scale sizes, the laser beam will also impinge on eddies of sizes smaller than its diameter. That will sometimes be the case for the uplink, but more frequently for the downlink, since the beam’s size increases over the propagation path. But for the downlink case, the additional increase of the laser beam’s size due to turbulence will be negligible, since the beam already has a very large size. Figure 5.4(a) shows the change of the shape of the beam only due to small eddies.

An approximate solution for the short-term beamspread can be found solely in [9]. The radius $\langle \rho_S \rangle$, defined by the distance where the intensity of the beam has decreased to $\exp[-1]$ of its maximum value, reads

$$\langle \rho_S^2 \rangle = \left(w_0 + \frac{\lambda L}{\pi w_0} \right)^2 + \left(\frac{\lambda L}{\pi \rho_0} \right)^2 \left[1 - 0.62 \left(\frac{\rho_0}{2w_0} \right)^{1/3} \right]^{6/5}. \quad (5.7)$$

For a Gaussian beam, this distance equals the standard deviation (which is the squareroot of the variance), as described in Sect. 2.3. The condition for the validity of this equation is the same as in 1a in the previous subsection.

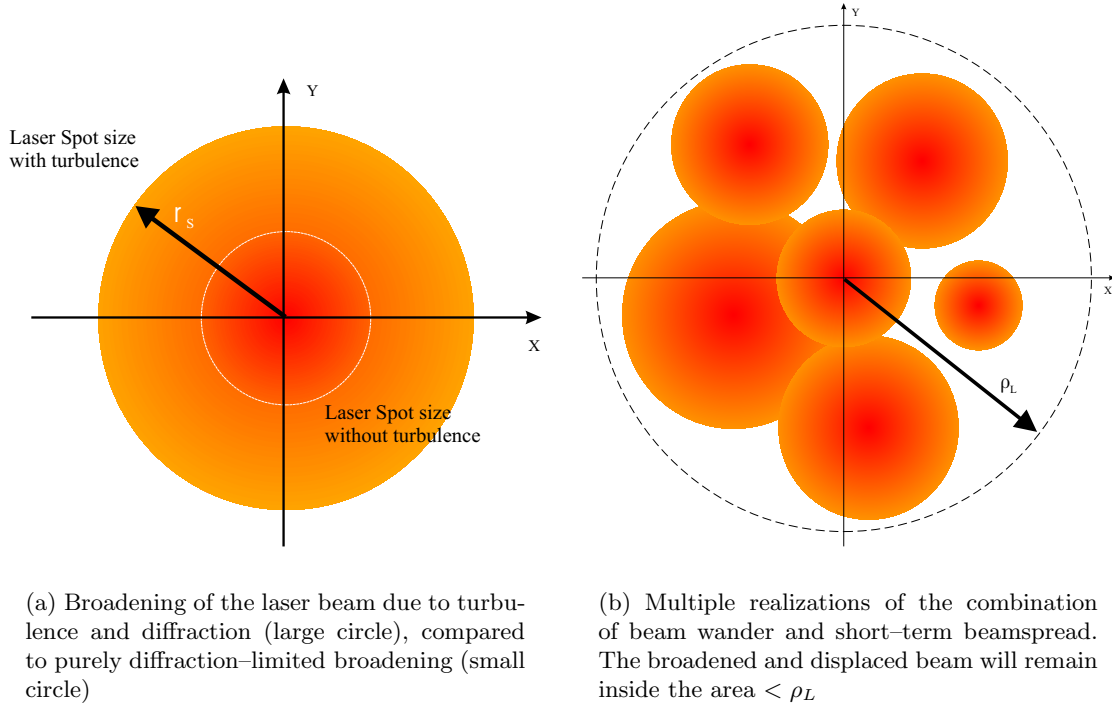


Figure 5.4: Intensity distributions of a laser beam after passing through turbulent atmosphere.

An analysis of (5.7) shows that the values for ρ_S lie at most 18% below the values for the long-term beamspread (next section), and that the form of the curves is approximately the same. Since I could not derive (5.7), this formula will not be used within further calculations. Other methods to obtain the short-term beamspread will be presented in the next section.

The short-term beamspread radius is more important for calculations of the system loss than the beam wander. The displacement of the center of the beam can be compensated by fast tracking systems, but the turbulent spreading of the beam can not be cancelled unless adaptive optics are applied at the transmitter and the receiver. Ishimaru has shown that after a few kilometers of propagation distance (3 to 10km), it makes no difference for the average on-axis irradiance whether a collimated or a focused beam is used [3].

5.5 Long-Term Beamspread

The combination of the beam wander (Sect. 5.3) and the short-term beamspread (Sect. 5.4) leads to the long-term beamspread [9],

$$\langle \rho_L^2 \rangle = \langle \rho_S^2 \rangle + \langle \rho_C^2 \rangle. \quad (5.8)$$

The notation “long-term” refers to the observation time that is much longer than for the “short-term” beamspread. While the short-term beamspread represents the additional broadening at a certain instant, the long-term beamspread represents the area where at least 84% of the intensity will be as long as the turbulent environment’s parameters do not change².

²These 84% are the amount of energy that is contained within $-\rho_L < r < \rho_L$.

These parameters are the structure parameter, and the inner and outer scale of turbulence. They obey *Taylor's frozen flow hypothesis*: The time it takes to blow the turbulent layer over the propagation path is much shorter than the time that is needed by turbulence to change its structure. This hypothesis can be approved easily: Looking at the sky, clouds pass the observer much faster than they change their form. In absolute values, the time constant for the change of turbulent parameters is on the order of a few seconds or minutes, while the time constant for motion due to wind is generally much smaller than one second.

Three possibilities of how the beam will react when propagating through turbulence have been presented in Sect. 5.3: The beam wanders and broadens, the beam wanders negligibly, or the beam breaks up into multiple patches. The particular form of the individual beam after being influenced by turbulence is unimportant for the long-term beamspread, since it mathematically represents an average over an infinite amount of realizations. The beam will remain inside a circular³ area with radius ρ_L . These behaviors can be seen in Fig. 5.4(a) and Fig. 5.4(b).

The energy of an unperturbed and a perturbed beam must be the same at any distance L . Therefore, the smaller the mean on-axis intensity of the perturbed beam will be, the larger must be its radius (or standard deviation),

$$\langle I(0) \rangle = A \frac{1}{\sqrt{2\pi}\sigma^2} \exp\left[-\left(\frac{|\vec{\rho}|}{\sigma}\right)^2\right] \Big|_{|\vec{\rho}|=0} = \frac{1}{\sqrt{2\pi}(\sigma/A)^2} \exp\left[-\left(\frac{|\vec{\rho}|}{\sigma}\right)^2\right] \Big|_{|\vec{\rho}|=0}, \quad (5.9)$$

where A is an arbitrary attenuation factor.

It is possible to obtain $\rho_L^2(L)$ by introducing a Gaussian function for the irradiance [6],

$$\langle I(\vec{r}, L) \rangle = \left(\frac{w(L)}{\rho_L(L)} \right)^2 \exp[-2(r/\rho_L(L))^2], \quad r = |\vec{r}|. \quad (5.10)$$

In this equation, $w(L)$ is the diffraction limited radius of the laser spot at the receiver. Using the mutual coherence function $\Gamma_{1,1}(\vec{r}, \vec{r}; L)$ from the Rytov approximation for the mean intensity $\langle I(\vec{r}, L) \rangle$, the long-term beamspread can then be calculated to be [6]

$$\langle \rho_L^2(L) \rangle = \begin{cases} w(L) \left(1 + 4.35 \int_0^L C_n^2(h) \left(1 - \frac{h}{L}\right)^{5/3} dh \cdot \right. \\ \quad \cdot \left. \left(\frac{2L}{kw^2(L)} \right)^{5/6} k^{7/6} L^{5/6} \right)^{1/2} & \dots \text{Uplink} \\ w(L) \left(1 + 4.35 \int_0^L C_n^2(h) \left(\frac{h}{L}\right)^{5/3} dh \cdot \right. \\ \quad \cdot \left. \left(\frac{2L}{kw^2(L)} \right)^{5/6} k^{7/6} L^{5/6} \right)^{1/2} & \dots \text{Downlink.} \end{cases} \quad (5.11)$$

This equation is plotted as a function of the initial beam waist in Fig. 5.5 (dash-dotted line), with $L = 450$ km, $\lambda = 1.55 \mu\text{m}$, and the H-V_{5/7} profile for $C_n^2(h)$.

The only difference between the uplink and the downlink case in (5.11) lies within the integrand. A closer analysis of the downlink case reveals that there is virtually no difference to the diffraction limited case. This behavior can be explained with the same arguments like in

³The circular area is a result of the isotropic form of the turbulence at a certain height.

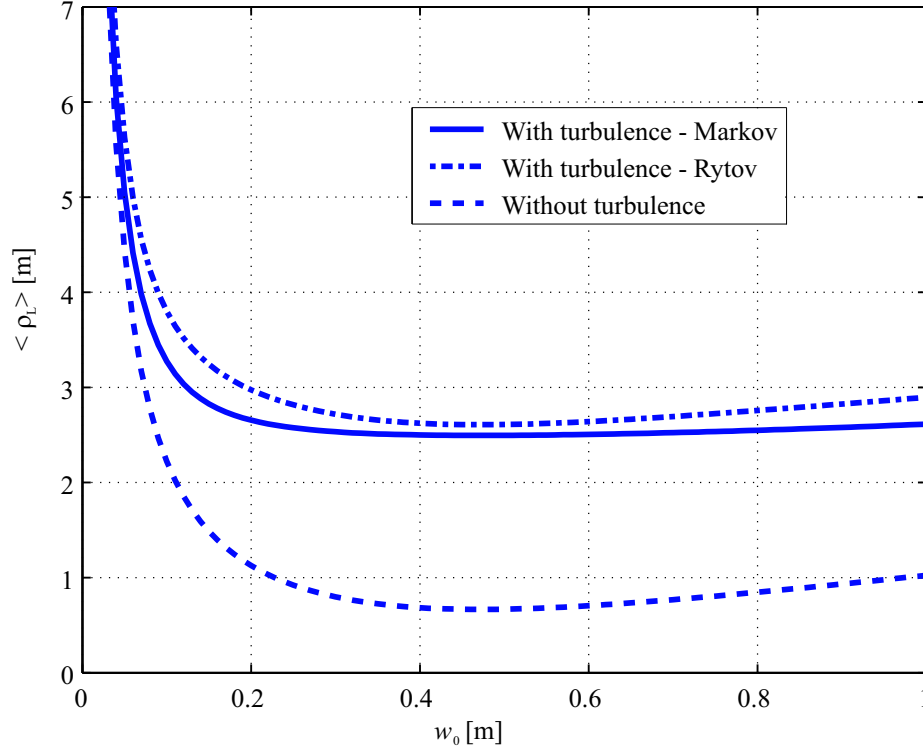


Figure 5.5: Different methods for deriving the long-term beamspread as a function of the transmitter's beam radius w_0 (uplink). The propagation distance is 450 km, and the wavelength $\lambda = 1.55 \mu\text{m}$ along with the Hufnagel–Valley_{5/7} profile are used.

Sect. 5.4, that is, the beam is already so large that a further increase of size due to turbulence is negligible.

In 1971, V. L. Mironov and S. S. Khmelevtsov found an expression for the relation between the average on-axis intensity of an unperturbed and a perturbed Gaussian laser beam [29]. They used the Markov approximation and involved degenerate hypergeometric functions ${}_1F_1$ (Kummer functions),

$$\begin{aligned} \frac{\langle I(L, 0) \rangle}{I_0(L, 0)} &= \frac{w(L)}{\langle \rho_L^2(L) \rangle} \\ &= 2 \int_0^\infty s \exp \left[-s^2 - \frac{1}{2} D_1 \left(L, \frac{2w_0}{g} s \right) \right] ds, \end{aligned} \quad (5.12)$$

where s is an auxiliary variable, and $g = \sqrt{1 + k^2 w_0^4 / L^2}$. The function $D_1(L, \frac{2w_0}{g} s)$ is defined by

$$D_1 \left(L, \frac{2w_0}{g} s \right) = 8.7 k^2 \kappa_m^{-5/3} \int_0^L C_n^2(h) \left[{}_1F_1 \left(-\frac{5}{6}, 1; -\left(\frac{w_0 \kappa_m}{g} \right)^2 s^2 \left(1 - \frac{h}{L} \right)^2 \right) - 1 \right] dh, \quad (5.13)$$

where $\kappa_m = 5.92/l_0$, and ${}_1F_1(a, b; z)$ is the Kummer function,

$$\begin{aligned} {}_1F_1(a, b; z) &= 1 + z \frac{a}{b} + \frac{z^2}{2!} \frac{a(a+1)}{b(b+1)} + \dots \\ &= \sum_{k=0}^{\infty} \frac{(a)_k}{(b)_k} \frac{z^k}{k!} \quad \text{with} \quad (a)_k = \prod_{l=0}^k (a+l), (a)_0 = 1. \end{aligned} \quad (5.14)$$

If $a < 0$ and either $b > 0$ or $b < a$, the series yields a polynomial with a finite number of terms. This is the case in (5.13). No comment about the range of validity of (5.12) has been made in [29]. This behavior is plotted as a solid curve in Fig. 5.5.

Fante postulated that two cases have to be distinguished calculating the long-term beam-spread [9]: Depending on the relation between the propagation distance L and the wavenumber $k = 2\pi/\lambda$, the inner scale of turbulence l_0 , and the structure parameter C_n^2 , one of the following equations has to be chosen:

$$\langle \rho_L^2 \rangle \approx \begin{cases} \left(w_0 + \frac{\lambda L}{\pi w_0} \right)^2 + \left(\frac{\lambda L}{\pi \rho_0} \right)^2 & \text{for } L \ll 1/(k^2 \tilde{C}_n^2 l_0^{5/3}) \\ \left(w_0 + \frac{\lambda L}{\pi w_0} \right)^2 + \frac{6.6 L^2 \int_0^L (1-h/L)^2 C_n^2(h) dh}{l_0^{1/3}} & \text{for } L \gg 1/(k^2 \tilde{C}_n^2 l_0^{5/3}). \end{cases} \quad (5.15)$$

The atmospheric coherence length ρ_0 in (5.15) was introduced in Sect. 5.3 and is defined by (5.6). To determine the equation that has to be used, the mean value \tilde{C}_n^2 (from (4.36)) has to be employed. For $\lambda = 1.55 \mu\text{m}$ and $l_0 = 8 \text{ mm}$, the right hand side of the condition for L becomes $8.7 \cdot 10^9 \text{ km}$, so the propagation distance will definitely lie within the range of validity for the first equation of (5.15). This equation is plotted in Fig. 5.5. It coincides with (5.12), and is labelled 'With Turbulence – Markov'. Therefore, it is assumed that (5.12) is also valid within this range.

In a report for the European Space Agency ("QSpace") [30], an approximation that involved *Fried's parameter* r_0 was used,

$$\begin{aligned} \langle \rho_L^2 \rangle &\approx w_0^2 + (\theta L)^2 = w_0^2 + \theta_{diff}^2 L^2 + \theta_{turb}^2 L^2 \\ &\approx \left(w_0 + \frac{\lambda L}{\pi w_0} \right)^2 + \left(\frac{\lambda L}{\pi r_0^2} \right)^2. \end{aligned} \quad (5.16)$$

The structure of (5.16) is the same as in (5.15), the only difference is the use of the Fried parameter instead of the atmospheric coherence length. The Fried parameter r_0 can be calculated by means of the atmospheric coherence length ρ_0 [31],

$$r_0 \approx 2.1 \rho_0, \quad (5.17)$$

which explains why (5.16) underestimates the atmospheric influence on the broadening of the beam. Using the Hufnagel–Valley_{5/7} turbulence profile for $C_n^2(h)$, r_0 takes on values around 19 cm. Measurements in a weakly turbulent environment confirm this value [32].

For comparison purposes, Fig. 5.5 also shows the diffraction limited beamradius as a dashed curve. This figure reveals that turbulence must not be neglected and will lead to a significant degradation of the irradiance at the receiver for the uplink.

The difference between the uplink and downlink scenario can be directly seen in Fig. 5.6. One transmitter is located at 0 km, the other transmitter at a height of 100 km. The initial beam waists of both transmitters are identical for each subfigure. For the long-term

beamspread, approximation (5.15) has been used. This figure clearly shows the additional beamspread for the uplink scenario, while for the downlink case, turbulent spreading can be neglected.

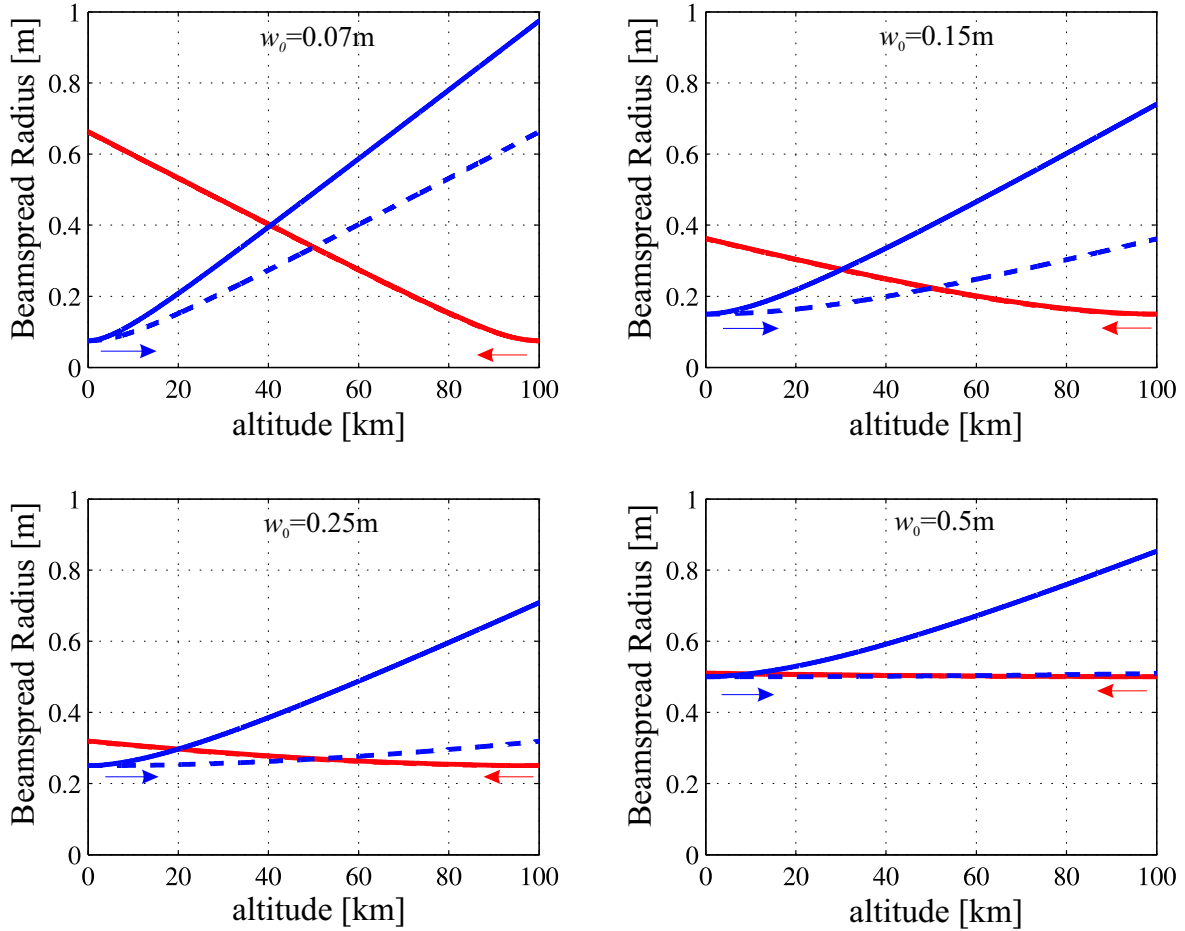


Figure 5.6: Direct comparison of the long-term beamspread of beams with varying beam radius w_0 for the uplink (blue) and downlink (red) scenario (the dashed line shows the diffraction limited beamsize, which has to be equal for the uplink and the downlink). The wavelength $\lambda = 1.55\text{ }\mu\text{m}$ and the Hufnagel–Valley_{5/7} profile are used.

5.6 Other Impacts

Beam spreading and beam wander are not the only impacts on a laser beam that passes through turbulence. There exist other phenomena, but they can be compensated easily or are of minor importance within optical communication, so they are mentioned here only briefly.

Angle of Arrival Fluctuations

The angle at which the transmitted beam impinges on the receiver's detection plane varies with time. If the arrival angle fluctuations were large, they resulted in an attenuation of the

intensity because of the radiation pattern of the receiving antenna. Calculations have shown that the turbulent arrival angle fluctuations are on the order of a few μrad for the uplink, while they are much larger for the downlink [3, 6].

A fast tracking device may be used to balance deviations in the arrival angle at the receiver. In this case, angle of arrival fluctuations will not lead to system degradation as long as the time constants of the tracking device are kept short enough (i.e., shorter than the fluctuation rate).

Scintillations

The wavefront is disturbed when it passes through turbulence, which leads to local changes of the phase of the electric field. When the wave impinges on the receiver, different parts of the wave interfere, resulting in a non-uniform distribution of the intensity. This effect is called *scintillation*, which is similarly used for variations of the irradiance in time and in space. Figure 5.7 shows a realization of scintillations for a field distribution that was initially Gaussian.

It can be shown that signal loss due to intensity scintillations will be around -1.26 dB for $\lambda = 1.55\text{ }\mu\text{m}$ and the H- $V_{5/7}$ profile, independent of the propagation distance (as long as the receiver is above turbulence) [34].

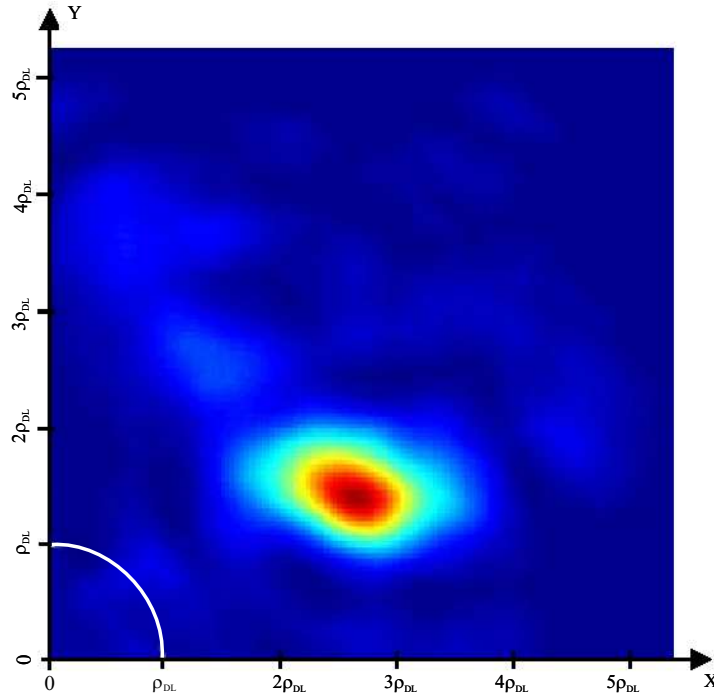


Figure 5.7: One realization of the intensity distribution of a Gaussian Beam after passing through turbulence (red = high intensity, blue = low intensity). The local variations of the irradiance are called scintillations. The center of the beam without turbulence lies in the lower left corner of the picture, and the part of the circle represents the diffraction limited spotradius, ρ_{DL} . This plot was obtained using PILab [33].

Chapter 6

System Loss

The results from Chapter 5 are used to calculate the link attenuation for free-space optical propagation through turbulence. The length of the propagation path is 450 km, which is a typical distance of an Earth–LEO (Low Earth Orbit) link. The wavelength $\lambda = 1.55 \mu\text{m}$ is used, and the characteristic of the structure parameter of turbulence $C_n^2(h)$ follows the Hufnagel–Valley_{5/7} profile. The modified atmospheric spectrum is used within all calculations.

6.1 Overall Path Attenuation

The atmospheric environment attenuates the intensity of the laser beam at the receiver’s antenna. The overall attenuation given in dB is a combination of the following parts:

$$A_{\text{atm}} = A_{\text{sbs}} + A_{\text{bw}} + A_{\text{scint}} + A_{\text{aoa}} + A_{\text{abs}} + A_{\text{sca}} \quad (6.1)$$

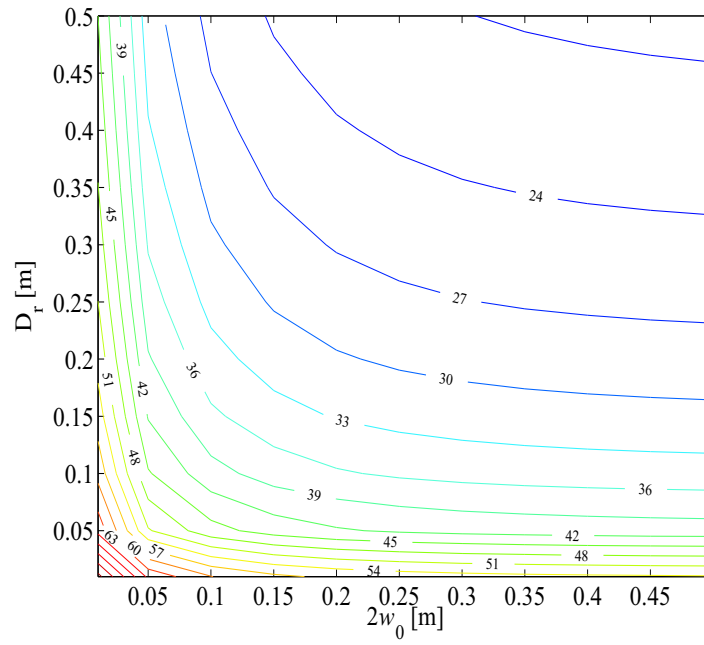
The attenuation due to the short-term beamsread A_{sbs} includes the diffraction (cf. Sect. 5.4), and A_{bw} represents the beam wander (cf. Sect. 5.3). These two impacts are discussed in detail on the following pages; it will be useful to subsume them to $A_{\text{turb}} = A_{\text{sbs}} + A_{\text{bw}}$. The attenuation due to scintillations, A_{scint} , will be approximately 1.26 dB, independent of the propagation distance [34]. It is assumed that the attenuation factor arising from angle of arrival fluctuations, A_{aoa} , is negligible (cf. Sect. 5.6). The term A_{abs} represents the absorption of energy by the chemical elements of the atmosphere (mainly water vapor). The last term, A_{sca} , stands for the attenuation due to scattering. Following Fig. 5.1, the attenuation due to absorption and scattering is on the order of 1 to 2 dB. It is assumed that no optical communication is possible if the atmosphere additionally attenuates the laser beam in a significant way.

The attenuation that results from the first two terms of (6.1) can be calculated using simple geometrical considerations. An antenna of constant size receives more power from a beam with a small diameter than from the same beam after broadening. Therefore, the size of the laser beam’s spot can be used to calculate the link attenuation,

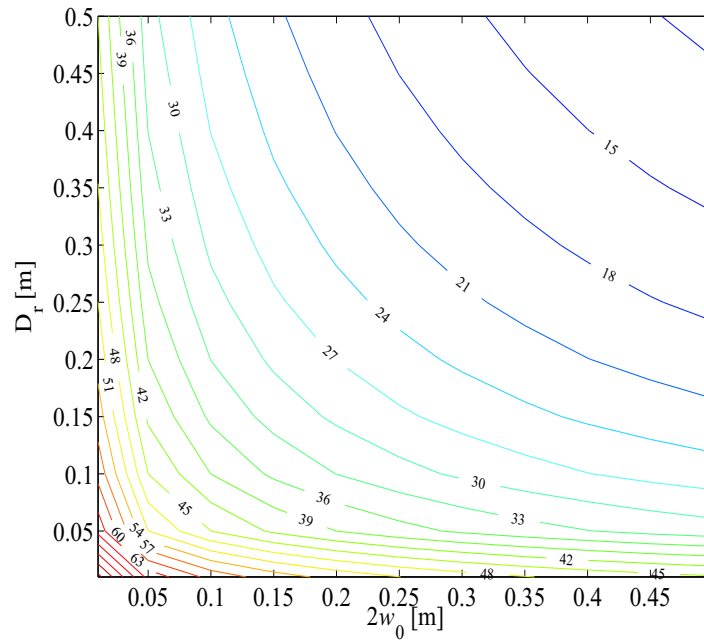
$$A_{\text{turb}} = 10 \log_{10} \left\{ \frac{D_r^2 \pi}{(2\rho_L)^2 \pi} \right\} = 20 \log_{10} \left(\frac{D_r}{2\rho_L} \right). \quad (6.2)$$

The diameter of the receiver’s antenna is given by D_r , and the diameter of the beam spot is twice the long-term beamsread radius, which is the (positive) squareroot of

$$\langle \rho_L^2 \rangle = \left(w_0 + \frac{\lambda L}{\pi w_0} \right)^2 + \left(\frac{\lambda L}{\pi \rho_0} \right)^2. \quad (6.3)$$



(a) Clear air atmospheric attenuation due to turbulence and diffraction.



(b) Attenuation due to diffraction only.

Figure 6.1: Link attenuation (in [dB]) as a function of the transmitter's beam diameter ($2w_0$) and of the diameter of the receiving aperture (D_r).

The Markov approximation method was used to derive this equation.

The beam waist radius at the transmitter is w_0 , and ρ_0 is the atmospheric coherence length, given by

$$\rho_0 = \left[1.46k^2 \int_0^L \left(1 - \frac{\eta}{L} \right)^{5/3} C_n^2(\eta) d\eta \right]^{-3/5}, \quad (6.4)$$

where k is the wavenumber.

The attenuation A_{turb} in dB is plotted in Fig. 6.1(a) as a function of the beam waist at the transmitter ($2w_0$) and of the diameter of the receiver's antenna (D_r). For small values of the beam waist, the attenuation is very high since the beam has a huge divergence. Very high attenuation factors can also be expected for small receiving antennas. In both cases, the ratio of the receiver's aperture and the actual spot size is very low.

Figure 6.1(a) reveals that increasing the beam's diameter at the transmitter beyond a certain width does not lead to a significant reduction of attenuation. For example, choosing $D_r = 0.2\text{m}$ and $2w_0 = 0.2\text{m}$, the attenuation is approximately 30.5 dB, and for $2w_0 = 0.4\text{m}$, the attenuation is 28.5 dB. Doubling the transmitter's beam diameter results in an improvement of only 2 dB. This behavior can be explained by the following analogy: The atmosphere can be seen as a large telescope with an aperture diameter that is determined by the Fried parameter¹ $r_0 = 2.1\rho_0$. Laser beams that are smaller than this "aperture" pass through turbulence without being influenced, while those beams with a larger diameter are affected by turbulence. A comparison with Fig. 6.1(b), where the attenuation due to diffraction only is plotted, shows the influence of the atmosphere. Increasing the transmitter's diameter in the diffraction limited case from $2w_0 = 0.2\text{m}$ to 0.4m results in a gain of 6 dB. This is insightful since the diameter of the transmitter to the power of two enters the formula to compute the attenuation (cf. (6.2) with ρ_{DL} instead of ρ_L).

Figure 6.2 shows the additional attenuation due to turbulence, i.e., the factor that is added to the diffraction limited attenuation. For very small diameters of the beam at the transmitter, the turbulent attenuation is negligible compared to the one from diffraction because the spot-size of the beam at the receiver is already quite large. The turbulence's impact increases with the size of the beam waist because the diffraction limited spotsize at the receiver decreases. For huge beam diameters, the turbulent attenuation becomes smaller again due to the fact that the spot size at the receiver has approximately the same size as at the transmitter (collimated beam), thus is also huge.

The results presented in Fig. 6.2 do not depend on D_r ,

$$\begin{aligned} A_{\text{turb}} - A_{DL} &= -10 \log_{10} \left(\frac{D_r^2}{(2\rho_L)^2} \right) - \left(-10 \log_{10} \left(\frac{D_r^2}{(2\rho_{DL})^2} \right) \right) \\ &= -20 \log_{10} \left(\frac{\rho_{DL}}{\rho_L} \right) = -10 \log_{10} \left(\frac{\rho_{DL}^2}{\rho_{DL}^2 + \rho_{\text{atm}}^2} \right) \\ &= 10 \log_{10} \left(1 + \frac{\rho_{\text{atm}}^2}{\rho_{DL}^2} \right). \end{aligned} \quad (6.5)$$

The diffraction limited spot radius is given by

$$\rho_{DL} = w_0 + \frac{\lambda L}{\pi w_0}, \quad (6.6)$$

¹For the Hufnagel-Valley_{5/7} profile, the Fried parameter is on the order of $\sim 19\text{ cm}$.

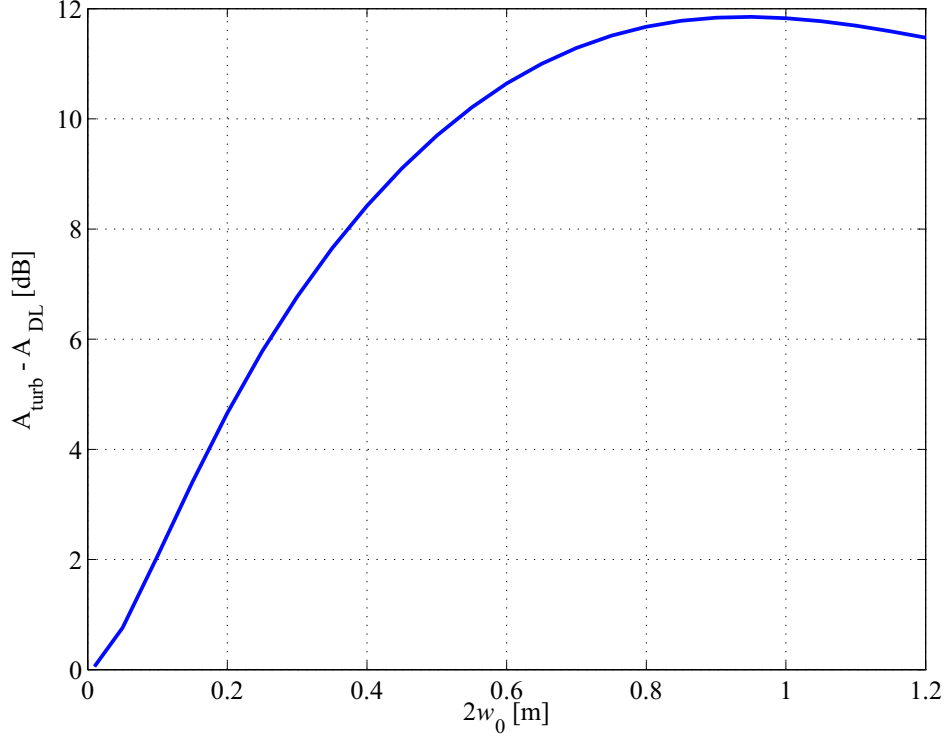


Figure 6.2: Increase of attenuation solely due to turbulence as a function of the initial beam diameter, $2w_0$ (A_{turb} = Attenuation due to the long-term beamspread, A_{DL} = Diffraction limited beamspread).

and the spot radius due to the atmospheric impact is

$$\rho_{\text{atm}} = \frac{\lambda L}{\pi \rho_0}. \quad (6.7)$$

6.2 Compensation of Atmospheric Impacts

It is possible to compensate for some atmospheric impacts on a laser beam. For example, the angle of arrival fluctuations (see Sect. 5.6) can be compensated by a fast tracking system. To estimate the time constant of this tracking system, a measure for the variations in time of the desired atmospheric impact has to be found. Assuming that the rate of change of atmospheric conditions mainly depends on the wind velocity (cf. Taylor's frozen flow hypothesis, Sect. 5.5), an approximation for the atmospheric time constant, τ_0 , is obtained by [35]

$$\tau_0 \approx \frac{r_0}{\bar{v}}. \quad (6.8)$$

In this equation, r_0 is the Fried parameter, and \bar{v} is the mean wind velocity². Inserting typical values for r_0 and \bar{v} (e.g., $r_0 = 0.2$ m, $\bar{v} = 50$ m/s)³, the atmospheric time constant can become

²The precise expression for τ_0 is given by the inverse *Greenwood frequency* that involves the wind velocity profile [35]. Using the Greenwood frequency, values for τ_0 are approximately 10 ms or more.

³The high value for \bar{v} results from typical wind velocities at heights from 10000 km to 13000 km, i.e., the region of *jetstreams*.

as low as 4 ms, which is an upper limit for the time constant of the tracking system.

It is also possible to eliminate the beam wander with the same tracking system, since the movement of the beam occurs with the same time constant. Figure 6.3 shows the remaining attenuation (solely due to beamspread) after cancelling the beam wander. Choosing 0.2 m

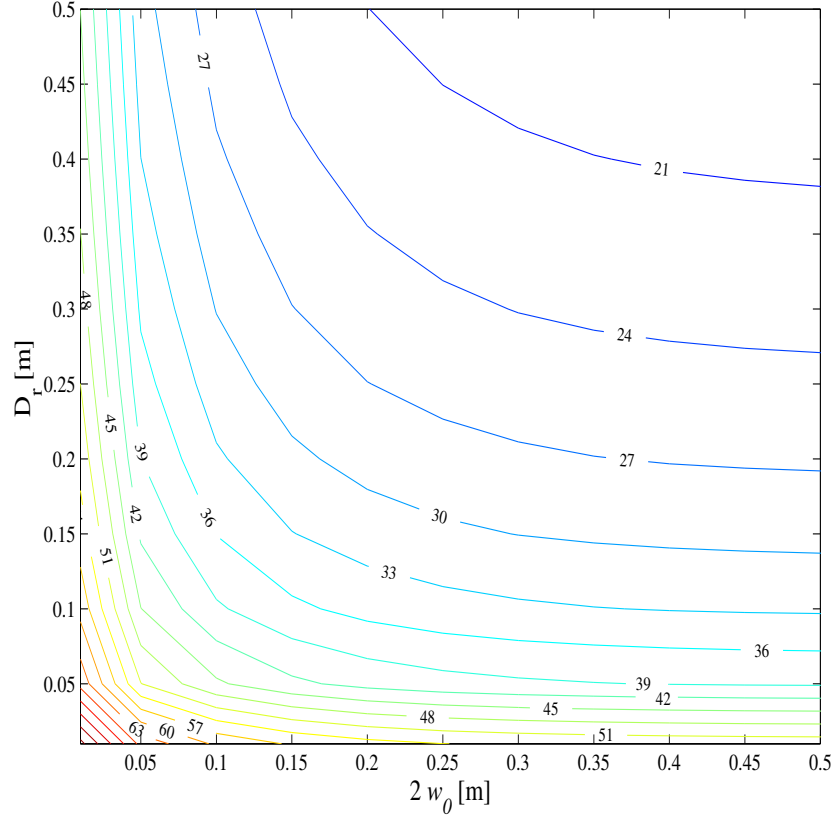


Figure 6.3: Link attenuation due to turbulence with compensated beam wander as a function of the transmitter beam diameter, $2w_0$, and the receiver's antenna size, D_r .

for the diameter of both the transmitter's beam and the receiver's antenna now leads to an attenuation factor of 29 dB. A comparison with the results from Fig. 6.1(a) reveals that cancelling the beam wander may lead to a gain in the intensity of approximately 2 dB. The real advantage of a fast tracking system lies beyond the (small) gain in intensity, as will be seen in the worst case scenario in the next section.

6.3 Assessment

In the previous subsections, the attenuation for an Earth-LEO link was calculated. Geometrical considerations led to the perception that a simple relation between the size of the broadened beam and the receiver's diameter yields the desired result.

The problem with this method is its dependency on the long-term beamspread, that is, on a factor that represents the average intensity of all possible realizations of beam wander and short-term beamspread (cf. Chap. 5). But the perturbed beam will never fill the whole area

defined by the long-term beamspread, so the attenuations calculated above are only mean values.

The dynamic range of the attenuation is defined by the best and worst case scenarios:

Best Case: Beam wander is negligible, i.e., the maximum of the intensity of the laser beam is in the middle of the receiver. This case is shown in Fig. 6.3. In addition, it is possible that the beam does not diverge to the maximum extent assumed in the definition of the short-term beamspread. These considerations lead to the conclusion that the attenuation will be only slightly above the values that are obtained for the diffraction limited case.

Worst Case: The beam wander reaches its maximum. It is possible to show, using the results from Chap. 5, that the maximum attenuation can be expected to be 15 dB higher than plotted in Fig. 6.1(a).

These considerations demonstrate that it is essential for an optical communication system to include a fast tracking system. The time constants of this system must be at least 10 ms or less.

Since the position of a LEO satellite is not fixed in space, the formulas for the attenuation are only valid if the receiving antenna is located at the zenith elevation angle (90°) directly above the transmitter. The angles of slant propagation paths have to be included for calculations of any other constellation. Generally speaking, any deviance from a vertical propagation path will lead to an increase of all mentioned impacts, thus to additional attenuations.

Appendices

Appendix A: Simulation Tools

To estimate the impact of the atmosphere on a laser beam, simulation tools can be used. The most challenging task is to simulate the random index of refraction. Different programs have been developed for various application areas. Most of these tools are available free of charge. They are generally build up as follows: A laser beam with well defined shape emerges from an aperture. The atmosphere is modelled by multiple phase screens [6] with infinitesimal small dilatation in the propagation direction, separated by areas where free-space propagation takes place. These layers only change the phase of the beam. (Note that the Markov approximation method decomposes the atmospheric propagation path in a similar way.)

A major difference of the simulation programs lies within the way the phase screens are approximated. An example of how the simulation of a Kolmogorov phase screen is done can be found in [36]. Most of these programs have been developed either for astronomic or for military tasks. Table 1 lists some simulation tools, together with a short description and web addresses for further information.

Name	Institution	Description & Adress
PILab	DLR (D)	PILab = Propagation and Imaging Lab; MATLAB [®] toolbox; Generates realizations of intensity distributions in the receiver's plane; Not available for public use http://www.dlr.de/KN/KN-DN/groups/optic/pilab/
WaveTrain	MZA (USA)	Approximates beam wander and beam spread among other things; Available free of charge (for US-companies only) http://www.mza.com/
CAOS	University of Florence (IT)	CAOS = Code for Adaptive Optics Systems; IDL-based; Tools for laser beam propagation do not exist yet; Available free of charge http://www.arcetri.astro.it/caos/
ALTM	Ontar Corp. (USA)	ALTM = Atmospheric Laser Turbulence Model; Simulates the link attenuation and reliability of an optical system for <i>horizontal</i> propagation paths, i.e., constant structure parameter; Prize: \$ 1,950.00 (28.03.2004) http://www.ontar.com/Software/product_ALTM.htm

Table 1: Simulation Tools for wave propagation in the atmosphere.

Symbols

c_0	...	Velocity of light, vacuum; $c_0 = 2.998 \cdot 10^8 \text{ ms}^{-1}$
$C_n^2(h)$...	Structure parameter of the refractive index [$\text{m}^{-2/3}$]
D_r	...	Diameter of the receiver's aperture [m]
$D_x(t, \tau)$...	Structure function of the parameter x [<i>depending on the unit of x</i>]
\vec{e}_i	...	Canonical basis
$\vec{\mathcal{E}}(\vec{x}; t)$...	Electric field vector in cartesian coordinates; time-dependent [Vm^{-1}]
$\vec{E}(\vec{x}, \omega)$...	Electric field vector in cartesian coordinates; frequency-dependent [Vm^{-1}]
f	...	Frequency [s^{-1}]
${}_1F_1(a, b; z)$...	Degenerate hypergeometric function (Kummer function) [1]
$G(\vec{s}, \vec{r}; z)$...	Green's function [m^{-1}]
$\vec{\mathcal{H}}(\vec{x}; t)$...	Magnetic field vector in cartesian coordinates; time-dependent; [Am^{-1}]
$\bar{I}(\vec{r}; z)$...	Average intensity [W m^{-2}]
\vec{k}	...	Wavevector; $\vec{k} = k_x \vec{e}_x + k_y \vec{e}_y + k_z \vec{e}_z$ [rad m^{-1}]
k	...	Wavenumber; $k = \mathbf{k} $
L	...	Overall propagation distance [m]
l_0	...	Inner scale of turbulence [m]
L_0	...	Outer scale of turbulence [m]
n	...	Index of refraction [1]
p	...	Pressure [$\text{Pa} = \text{kg m}^{-1}\text{s}^{-2}$]
\vec{r}	...	Radius in the plane perpendicular to the propagation direction [m]
r_0	...	Fried parameter [m]
$R(z)$...	Radius of the phase front curvature of a Gaussian beam [m]
R_e	...	Reynoldsnumber [1]
t	...	Time [s]
T	...	Temperature [K]
$u(\vec{x})$...	Location-dependent amplitude of the electric field [Vm^{-1}]
\vec{v}	...	Wind velocity [m/s]
v	...	Pseudo-windspeed [m/s]
\bar{v}	...	Mean wind velocity [m/s]
v_{ph}	...	Phase Velocity [m/s]
v_{gr}	...	Group Velocity [m/s]
w_0	...	Gaussian beam waist radius [m/s]
$w(z)$...	Beam radius of a Gaussian beam at distance z from the transmitter [m]
\vec{x}	...	Cartesian vector; $\vec{x} = x\vec{e}_x + y\vec{e}_y + z\vec{e}_z$ [m]
z_0	...	Confocal parameter; [m]

$\delta(x)$...	Delta-distribution [1]
ε	...	Electric Permittivity; $\varepsilon_0 = 8.854 \times 10^{-12} \text{ AsV}^{-1}\text{m}^{-1}$ (vacuum) ε_r = Relative electric permittivity [1]; $\varepsilon = \varepsilon_r \varepsilon_0$
$\Gamma_{m,n}$...	Moment of a stochastic field of the order $m + n$ [<i>unit depends on order</i>]
$\gamma(\vec{r})$...	Complex degree of coherence [1]
λ	...	Wavelength; $\lambda_0 = c_0/f$; [m]
μ	...	Magnetic Permeability; $\mu_0 = 4\pi \times 10^{-7} \text{ VsA}^{-1}\text{s}^{-1}$ (vacuum) μ_r = Relative magnetic permeability [1]; $\mu = \mu_r \mu_0$
ν	...	kinematic viscosity [m^2/s]
$\Phi_n(\kappa)$...	Spectrum of the fluctuations of the refractive index [$\text{rad}^{-11/3}\text{m}^3$]
ρ_0	...	Atmospheric coherence length [m]
ρ_C	...	Beam Wander [m]
ρ_{DL}	...	Diffraction-limited beamspread [m]
ρ_S	...	Short-term beamspread [m]
ρ_L	...	Long-term beamspread [m]
σ_1	...	Scintillation index [1]
τ_0	...	Atmospheric time constant [s]
$2\theta_0$...	Aperture angle of a Gaussian beam]rad]
ω	...	Angular frequency [rad s^{-1}]

Bibliography

- [1] R. Sasiela, *Electromagnetic Wave Propagation in Turbulence*. Berlin Heidelberg New York: Springer, 1993.
- [2] H. Kogelnik and T. Li, "Laser beams and resonators," *Proceedings of the IEEE*, Vol. 54, no. 10, pp. 1312–1329, 1966.
- [3] J. W. Strohben, S. F. Clifford, M. E. Gracheva, A. S. Gurvich, S. S. Kashkarov, V. V. Pokasov, A. Ishimaru, J. H. Shapiro, J. L. Walsh, and P. B. Ulrich, "Laser beam propagation in the atmosphere," in *Topics in Applied Physics*, J. W. Strohben, Ed. Berlin: Springer-Verlag, 1978, Vol. 25.
- [4] S. M. Rytov, Y. A. Kravtsov, and V. I. Tatarskii, "Wave propagation through random media," in *Principles of statistical radiophysics*. Berlin: Springer-Verlag, 1989, Vol. 4.
- [5] U. Frisch, Ed., *Turbulence: The Legacy of A.N. Kolmogorov*. Cambridge: Cambridge University Press, 1995.
- [6] L. C. Andrews and R. L. Phillips, *Laser Beam Propagation Through Random Media*. SPIE - The International Society for Optical Engineering, 1998.
- [7] H. T. Yura, "Short-term average optical-beam spread in a turbulent medium," *Journal of the Optical Society of America*, Vol. 63, no. 5, pp. 567–572, 1973.
- [8] E. Azoulay, V. Thiermann, A. Jetter, A. Kohnle, and Z. Azar, "Optical measurement of the inner scale of turbulence," *Journal of Physics D: Applied Physics*, Vol. 21, pp. 41–44, 1988.
- [9] R. L. Fante, "Electromagnetic beam propagation in turbulent media," *Proceedings of the IEEE*, Vol. 63, no. 12, pp. 1669–1692, 1975.
- [10] A. M. Prokhorov, F. V. Bunkin, K. S. Gochelashvily, and V. I. Shishov, "Laser irradiance propagation in turbulent media," *Proceedings of the IEEE*, Vol. 63, no. 5, pp. 790–811, 1975.
- [11] R. L. Fante, "Electromagnetic beam propagation in turbulent media: An update," *Proceedings of the IEEE*, Vol. 68, no. 11, pp. 1424–1443, 1980.
- [12] S. Kempler. (2004, March) Ozone and atmospheric structure. [Online]. Available: http://daac.gsfc.nasa.gov/campaign_docs/atm_chem/atmospheric_structure.html
- [13] M. Jeschke. (2004, March) Zusammensetzung und geschichtliche Entwicklung der Erdatmosphäre (in german). [Online]. Available: http://private.freepage.de/cgi-bin/feets/freepage_ext/41030x030A/rewrite/marjano/Atmos.htm

- [14] J. H. Peters. (2004, March) Kármánsche Wirbelstrasse (in german). [Online]. Available: <http://www.philippi-trust.de/hendrik/braunschweig/wirbeldoku/karman.html>
- [15] V. V. Voitsekhovich, “Outer scale of turbulence: Comparison of different models,” *Journal of the Optical Society of America A*, Vol. 12, no. 6, pp. 1346–, 1995.
- [16] A. Tokovinin, A. Ziad, F. Martin, R. Avila, J. Borgnino, R. Conan, and M. Sarazin, “Wavefront outer scale monitoring at la scilla,” 1998. [Online]. Available: <http://citeseer.ist.psu.edu/tokovinin98wavefront.html>
- [17] H. Weinrichter and F. Hlawatsch, *Stochastische Grundlagen nachrichtentechnischer Signale*. Springer, 1991.
- [18] H. J. Dirschmid, *Mathematische Grundlagen der Elektrotechnik*, 1st ed. Braunschweig: Vieweg, 1986.
- [19] A. Ishimaru, “Wave propagation and scattering in random media and rough surfaces,” *Proceedings of the IEEE*, Vol. 79, no. 10, pp. 1359–1366, 1991.
- [20] A. N. Kolmogorov, “The local structure of turbulence in an incompressible viscous fluid for very large reynolds numbers,” *Doklady Acad. Sci. USSR*, Vol. 30, no. 4, pp. 301–305, 1941.
- [21] A. Zilberman, E. Golbraikh, and N. S. Kopeika, “Validity of kolmogorov turbulence at higher elevations,” in *Proceedings of SPIE: Free-Space Laser Communication Technologies XVI*, Vol. 5338. Lexington: SPIE Press, 2004.
- [22] M. Adcock, N. Wooder, and V. Kluckers. (2004, March) Introduction to SCIDAR. [Online]. Available: http://op.ph.ic.ac.uk/scidar/scidar_in.html
- [23] N. Wooder and V. Kluckers. (2004, March) SCIDAR measurements at ICSTM. [Online]. Available: <http://op.ph.ic.ac.uk/scidar/results.html>
- [24] A. Kudryashov *et al.* (2003, July) Shack-Hartmann Wavefront Sensor for Laser Beam Analysis. [Online]. Available: <http://www.laser.ru/adopt/Science/sens/sensor.htm>
- [25] Austro Control. (2004, March) Austro Control Wetter Lexikon (in german). [Online]. Available: <http://www.austrocontrol.at/weather/lexfull.html>
- [26] F. H. Ruggiero and D. A. DeBenedictis. (2003, August) Forecasting Optical Turbulence from Mesoscale Numerical Weather Prediction Models. [Online]. Available: http://www.hpcmo.hpc.mil/Htdocs/UGC/UGC02/paper/frank_ruggiero1_paper.pdf
- [27] W. K. Pratt, *Laser Communication Systems*, 1st ed. New York: John Wiley & Sons, Inc., 1969.
- [28] V. I. Klyatskin and A. I. Kon, “On the displacement of spatially-bounded light beams in a turbulent medium in the markovian-random-process appoximation,” *Radiophysics and Quantum Electronics*, Vol. 15, pp. 1056–1061, 1972.
- [29] V. L. Mironov and S. S. Khmelevtsov, “Broadening of a laser beam propagating in a turbulent atmosphere along inclined routes,” *Radiophysics and Quantum Electronics*, Vol. 15, pp. 567–571, 1972.

- [30] M. Aspelmeyer, H. R. Böhm, C. B. R. Kaltenbaek, M. Lindenthal, J. Petschinka, T. Jennewein, R. Ursin, P. Walther, A. Zeilinger, M. Pfennigbauer, and W. Leeb, “Quantum communications in space (“QSpace”),” Institut für Nachrichtentechnik und Hochfrequenztechnik, TU Wien,” European Space Agency Contract Report, ESTEC, Contract No. 16358/02/NL/SFe, Final Report, 2003.
- [31] D. L. Fried, “Statistics of a geometric representation of wavefront distortion,” *Journal of the Optical Society of America*, Vol. 55, no. 11, pp. 1427–1435, 1965.
- [32] A. R. Weiss, S. Hippler, M. E. Kasper, N. J. Wooder, and J. C. Quartel, “Simultaneous measurements of the fried parameter r_0 and the isoplanatic angle θ_0 using scidar and adaptive optics - first results,” in *Marrakech Site 2000 Conference Proceedings*, Marrakech, 2000.
- [33] R. Juengling, “Simulation gerichteter Ausbreitung optischer Wellen in turbulenter Atmosphäre (in german),” Diploma Thesis, Westfälische Wilhelms-Universität, Münster, 2001.
- [34] G. Gilbert and M. Hamrick, “Practical quantum cryptography: A comprehensive analysis (part one),” MITRE,” Technical Report, 2000.
- [35] V. W. S. Chan, J. H. Shapiro, and F. N. C. Wong, “Atmospheric optical communications – architecture, system design and concept demonstration of a battlefield agile-beam optical communication system,” 2004. [Online]. Available: http://www.darpa.mil/mto/stab/kickoff/stab_mit.pdf
- [36] M. van Dam. (2004, March) Simulation of adaptive optics systems. [Online]. Available: <http://cfao.ucolick.org/pubs/presentations/aosummer03/vanDam.pdf>